REVIEW ARTICLE

Check for updates

Carbon-supported platinum-based electrocatalysts for alkaline hydrogen evolution

Qiuyue Yang,†[ab] Jilan Zeng,†[ab] Guowei Yang,[ab] Xinran Sun,[ab] Xiahui Lin,[ab] Kunlong Liu, ✚[*ab] Jiayi Chen,*[ab] Sibo Wang ✚ *[ab] and Xue Feng Lu ✚ *[ab]

Water electrolysis hydrogen production technology directly generates high-purity hydrogen through electrochemical water splitting, serving as a key technology for achieving zero-carbon emission hydrogen production. Alkaline water electrolysis demonstrates marked advantages in efficiency and rapidly developing anode catalysts in an alkaline medium. Nevertheless, the sluggish kinetics of the hydrogen evolution reaction (HER) at the cathode in an alkaline environment constitute a fundamental bottleneck that restricts the extensive application of this technology. Platinum, serving as the benchmark catalyst for the HER, is limited in its large-scale development due to its scarcity and high cost. In comparison, carbon-supported platinum-based catalysts exhibit exceptional HER catalytic activity and stability, driven by their unique electronic architecture and the synergistic effect with the support. In this review, we comprehensively examine the latest progress of carbon-supported platinum-based materials for the alkaline HER, summarize the factors contributing to the slow kinetics of the HER in an alkaline environment, and then focus on the strategies for modifying the carbon substrate and synthesizing carbon-supported platinum-based nanomaterials. Finally, the review critically evaluates existing challenges and proposes targeted research directions to advance Pt-based electrocatalysts for practical alkaline hydrogen evolution systems.

Broader context

Amid global carbon neutrality efforts, hydrogen, particularly green hydrogen, is poised to play a pivotal role, with demand projected to surge sixfold by 2050. Alkaline water electrolysis, a cost-effective and stable hydrogen production technology, stands as a key enabler of this transition. Yet its widespread adoption is hampered by the sluggish kinetics of the alkaline hydrogen evolution reaction (HER). While platinum remains the benchmark HER catalyst, its scarcity and expense drive the search for high-performance, scalable alternatives. Carbon-supported Pt-based catalysts, benefiting from tailored electronic structures and carrier interactions, exhibit exceptional activity and durability, offering a viable pathway to industrial-scale implementation. This review examines recent progress in such materials, analyzes the origins of alkaline HER's kinetic limitations, and outlines strategic modifications to carbon supports and Pt nanostructures—critical steps toward unlocking the full potential of green hydrogen and achieving global decarbonization.

1. Introduction

The deepening of the energy crisis has prompted human society to pay more attention to renewable energy, develop clean energy, and respond to global carbon neutrality policies.[1–3] Hydrogen, as a new type of clean energy source, is considered to be a new player in solving the energy crisis to a great extent due to its advantages of remarkable energy density

and pollution-free combustion. The Hydrogen Council estimates that the total investment in the hydrogen energy sector worldwide is expected to reach $500 billion by 2030, with the demand for clean hydrogen reaching 75 million tons, which highlights the necessity of highly efficient hydrogen production technologies.[4,5] H_2 is predominantly classified into green hydrogen, gray hydrogen, and blue hydrogen. Compared with gray hydrogen and blue hydrogen produced by coal combustion or steam methane reforming, green hydrogen created *via* water electrolysis using electrical energy (such as wind power or solar energy) is favored due to its clean, efficient, and sustainable carbon-neutral hydrogen production process.[6,7]

While water electrolysis boasts significant merits for green hydrogen production, its industrial-scale deployment remains constrained by persistent challenges, including excessive

[a] State Key Laboratory of Chemistry for NBC Hazards Protection, College of Chemistry, Fuzhou University, Fuzhou 350116, China. E-mail: klliu@fzu.edu.cn, jiayi9236@fzu.edu.cn, sibowang@fzu.edu.cn, luxf@fzu.edu.cn
[b] State Key Laboratory of Photocatalysis on Energy and Environment, College of Chemistry, Fuzhou University, Fuzhou 350116, P. R. China
† These authors contributed equally to this work.

energy input, prohibitive capital expenditure, and suboptimal system efficiency.[2,8] Water electrolysis involves the hydrogen evolution reaction (HER) at the cathode and the oxygen evolution reaction (OER) at the anode, where the efficient progression of the cathode HER is a critical link for realizing green hydrogen production. However, alkaline HER systems face unique challenges due to the characteristics of the medium. In an alkaline environment, the dissociation kinetics of water molecules are slow, and the presence of hydroxide ions (OH^-) significantly alters the reaction pathway and adsorption behavior of intermediates, requiring catalysts to possess excellent dual capabilities for water dissociation and hydrogen

Qiuyue Yang received her BSc degree in 2023 from Hubei University. She is currently an MSc student under the supervision of Prof. Xue Feng Lu at Fuzhou University. Her research interest focuses on the design and synthesis of advanced electrocatalysts for electrochemical hydrogen evolution and carbon dioxide reduction.

Qiuyue Yang

Jilan Zeng received her BSc degree in 2023 from Chongqing Normal University. She is currently an MSc student under the supervision of Prof. Xue Feng Lu at Fuzhou University. Her research interest focuses on the design and synthesis of Co/Mn-based electrocatalysts for water electrolysis.

Jilan Zeng

Dr Kunlong Liu received his BS degree in Optical Information Science and Technology from Northwestern Polytechnical University in 2013 and his PhD degree in 2020 from Xiamen University under the guidance of Profs. Nanfeng Zheng and Gang Fu. During 2020–2022, he worked as a postdoctoral scholar at Xiamen University. He moved to Fuzhou University in 2022. His research focuses on the surface and interface chemistry of photo(electro)catalytic overall water splitting.

Kunlong Liu
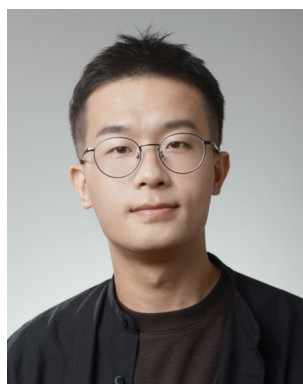
Dr Jiayi Chen is currently a faculty member at the State Key Laboratory of Photocatalysis on Energy and Environment, Fuzhou University, China. He received his BS (2014) and MS (2017) degrees from Lanzhou University, and PhD (2020) degree from the University of Wollongong, Australia. He conducted postdoctoral research at the National University of Singapore from 2021 to 2024. His research focuses on the mechanistic design of electrocatalytic systems for water splitting and CO_2/CO reduction.

Jiayi Chen

Dr Sibo Wang is a Professor at the State Key Laboratory of Photocatalysis on Energy and Environment, Fuzhou University. He obtained his PhD degree from Fuzhou University in 2016 and then went to Nanyang Technological University for postdoctoral research. In 2020, he was recruited at Fuzhou University as a Professor through the Global Recruitment Program of China. His main research interests are photocatalytic CO_2 reduction, CH_4 conversion and water splitting.

Sibo Wang

Dr Xue Feng LU is currently a full professor at the State Key Laboratory of Photocatalysis on Energy and Environment, Fuzhou University, China. He obtained his PhD degree from Sun Yat-sen University in 2017. He carried out postdoctoral research at Nanyang Technological University, Singapore and The Hong Kong Polytechnic University from August 2017 to July 2022. His research interests focus on the design and synthesis of advanced functional materials towards electrochemical energy storage and conversion.

Xue Feng Lu

adsorption/desorption. Although research on non-noble metal catalysts has made certain progress in recent years, demonstrating hydrogen evolution performance comparable to that of platinum (Pt)-based catalysts, their rapid performance degradation and insufficient structural stability during actual device operation directly restrict their widespread industrial application.[9] Therefore, in large-scale industrial hydrogen production, Pt-based catalysts remain the core elements to ensure the high current density and low-energy consumption operation of electrolyzers, and their irreplaceable performance makes them the cornerstone of industrial application for alkaline HER systems. Pt has been recognized as the benchmark HER catalyst because of its optimal hydrogen binding energy (HBE), which positions it near the apex of the HER activity volcano plot. This plot correlates experimental exchange current densities (j_0) with theoretical Gibbs free energy (ΔG_{H^*}) values, revealing a distinct "volcano-shaped" relationship: the HER activity peaks when HBE approaches that of Pt, while deviations in HBE (either stronger or weaker) lead to a dramatic decline in activity.[10,11] The Sabatier principle explains that while excessively weak HBE hinders hydrogen adsorption, overly strong HBE impedes hydrogen desorption, with both extremes limiting reaction efficiency.[12–14]

Nevertheless, the inherent scarcity of Pt and its fluctuating price dynamics fundamentally constrain the large-scale commercialization and economic feasibility of alkaline water electrolysis. Besides, under the alkaline HER conditions, the dissolution loss of active components and agglomeration-induced deactivation of Pt catalysts are the core issues restricting the long-term efficient operation of the catalytic system.[15] From a materials chemistry perspective, the dissolution mechanism of Pt exhibits multi-factor synergy. Specifically, under high potential, OH^- as a strong nucleophile directly attacks the Pt lattice, promoting its oxidation to form soluble hydroxides such as $Pt(OH)_4$. Meanwhile, the coordination compounds formed by OH^- and Pt significantly reduce the activation energy of the dissolution reaction, accelerating the loss of active sites. Additionally, the strong adsorption of H* on the Pt surface induces lattice distortion, destroying the crystal structure stability and further exacerbating Pt dissolution.[16,17] The agglomeration of Pt nanoparticles (NPs) stems from the coupling of thermodynamic driving forces and environmental factors. First, the high surface energy of small-sized Pt NPs triggers Ostwald ripening, promoting particle size homogenization through a "dissolution–deposition" mechanism. Second, corrosion of the support material in alkaline environments disrupts the anchoring structure of Pt NPs, leading to migration and agglomeration of active components. Third, the ordered reconstruction of interfacial water molecules alters the electrostatic repulsion between NPs, facilitating their collision and fusion. Finally, the mechanical impact of H_2 bubbles generated during the HER also accelerates the agglomeration of Pt NPs.[18] These stability issues highlight the need to break through the traditional single-performance improvement paradigm and construct an "activity-stability-economy" trinity design strategy for alkaline HER catalysts. On the basis of ensuring the intrinsic catalytic activity of noble metals, it is urgent to achieve atomic-level dispersion of Pt and inhibit particle agglomeration through means such as nanostructure regulation, support interface engineering, and composite catalytic system design. Meanwhile, enhancing corrosion resistance *via* interfacial electronic structure optimization can ultimately achieve synergistic enhancement of catalytic efficiency and material utilization.[19,20]

Noble metals Pt possess superior surface free energy, usually loading on support during synthesis and reaction processes to enhance dispersion and prevent aggregation.[21] Carbon-based materials are generally recognized as compelling and intriguing catalyst supports. Compared with other supports such as metal oxides, they feature high electrical conductivity, excellent chemical stability, and tuneable surface electronic structures. Firstly, the highly conductive framework facilitates charge transfer to the catalyst surface. In contrast, metal oxide supports (*e.g.*, Ni-based) usually have poor conductivity, which easily becomes a bottleneck for charge transfer. Secondly, the extensive specific surface area and porous architecture enhance active site exposure while optimizing mass transport efficiency. However, Ni-based supports have a small specific surface area and irregular pore structures, leading to the aggregation of Pt particles and a reduction in the number of active sites.[22] Thirdly, excellent electrochemical stability is maintained over a wide potential window, demonstrating tolerance to harsh alkaline electrolytic environments. Finally, defect engineering and elemental doping enable precise electronic structure modulation through strong metal–support interactions (SMSI), offering multidimensional strategies for catalytic performance optimization.[23] Moreover, the surface functional groups of carbon supports can tune the adsorption energy of Pt, optimizing the adsorption and desorption of reaction intermediates, whereas the surface properties of metal oxide supports are difficult to regulate.[24,25] However, carbon materials are prone to corrosion in alkaline media, leading to poor stability.[26] The corrosion mechanism of carbon mainly originates from electrochemical oxidation, nucleophilic attack of OH^-, galvanic corrosion, and dissolution–deposition effects. Under high potential, OH^- generates $^{\bullet}OH$ radicals that attack the carbon skeleton, oxidizing it into oxygen-containing functional groups such as carbonyl and carboxyl, which eventually decompose into soluble carbonates. OH^- also directly attacks defect sites on carbon, weakening the skeleton stability.[27] When carbon supports metal catalysts, the potential difference between the metal and carbon forms a micro-battery, with carbon acting as the anode to accelerate oxidation. Additionally, the metal may catalyze the generation of strong oxidizing species to indirectly corrode carbon. Furthermore, carbonates formed by corrosion redeposit with changes in pH or potential, blocking carbon pores. Meanwhile, the collapse of carbon nanostructures causes instability and aggregation of metal particles.[28]

Currently, significant endeavors have been committed to deciphering the mechanistic insight and application boundaries of Pt-based electrocatalysts in alkaline HER. These scholarly endeavors have been systematically analyzed in multiple authoritative reviews that map the evolution trajectory of this field. For example, Liu *et al.* systematically investigated the electronic structure–activity correlation mechanism in carbon-supported noble metal catalysts and proposed to improve the slow HER kinetics by optimizing the
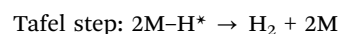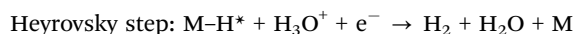
synthesis strategy and structural characterization.[12] Sui *et al.* comprehensively reviewed the influence of support materials on noble metal single-atom catalysts (SACs), elaborating the critical roles of carriers—including anchoring effects, SMSI, and synergistic catalytic mechanisms—thereby establishing a novel theoretical paradigm to address key challenges in the scalable application of noble metal SACs.[29] Ma *et al.* critically delineated mechanistic modulation approaches to overcome kinetic limitations in alkaline HER, while establishing design principles for advanced Pt-based electrocatalysts with record-breaking efficiency.[8] Zhang *et al.* conducted a critical investigation into the mechanisms underlying HER activity enhancement, systematically elucidating strategies for modulating the interactions between active sites and reaction intermediates.[1] Furthermore, recent advances in support materials are categorized and elaborated in detail, focusing on their anchoring mechanisms.[30]

The aforementioned review has comprehensively explored critical areas, including synthesis optimization, the HER mechanism, the structure–activity relationship, and practical applications. Notably, despite numerous investigations revealing that the HER kinetics in alkaline media exhibit a much slower rate, with a 2–3 orders-of-magnitude decrease relative to the kinetics in acidic media, a clear and consistent understanding of this phenomenon remains elusive. Consequently, we commence by summarizing the latest research findings regarding the sluggish reaction kinetics of the alkaline HER, aiming to shed light on this long-debated scientific conundrum. Building on this foundation, we methodically examine recent progress in carbon-supported Pt nanomaterials, focusing on three interconnected dimensions: strategic modifications of carbon matrix support, innovative synthesis approaches for carbon-supported Pt nanomaterials, and their resulting alkaline HER electrocatalytic

performance in terms of activity, stability, and reaction kinetics. Finally, we critically evaluate the prevailing challenges within this field, such as limited understanding of alkaline interfacial processes and scalability constraints of advanced catalysts, while proposing feasible research directions grounded in experimental and theoretical advancements to guide the development of next-generation alkaline HER electrocatalysts (Fig. 1).

2. Key factors of the slow kinetics of the HER under alkaline conditions

As a prototypical two-electron transfer process, the HER encompasses three key elementary steps: the Volmer step, the Heyrovsky step, and the Tafel step. Notably, the overall HER exhibits distinct characteristics depending on the electrolyte environment. In acidic media, the reaction involves protons, whereas in alkaline media, hydroxide ions play a crucial role:[19,31,32]

In acid:

$$\text{Volmer step: } H_3O^+ + e^- + M \rightarrow M–H^* + H_2O$$

$$\text{Heyrovsky step: } M–H^* + H_3O^+ + e^- \rightarrow H_2 + H_2O + M$$

$$\text{Tafel step: } 2M–H^* \rightarrow H_2 + 2M$$

In alkaline:

$$\text{Volmer step: } H_2O + e^- + M \rightarrow M–H^* + OH^-$$

$$\text{Heyrovsky step: } M–H^* + H_2O + e^- \rightarrow H_2 + OH^- + M$$

$$\text{Tafel step: } 2M–H^* \rightarrow H_2 + 2M$$

where M represents the hydrogen adsorption sites and the M–H* denotes the adsorbed hydrogen intermediate. The initial stage of this reaction is the Volmer reaction, where hydronium ions (or water molecules) and electrons interact to generate an H* intermediate on the catalyst surface. Following this, H_2 is generated through the Heyrovsky step, the Tafel step, or a combination of both. More precisely, under conditions of low H* coverage, the Heyrovsky reaction dominates the hydrogen evolution process. It entails the interaction between an H* intermediate and a water molecule, ultimately leading to the form of H_2. Conversely, as the surface coverage of H* intermediates increase, the Tafel reaction becomes favorable when an adequate amount of H* accumulates on the catalyst. This reaction involves the combination of two H* species, followed by the desorption of H_2 from the catalyst surface.[31,33]

As is well known, the reaction rate of the HER in alkaline media is generally 2–3 orders of magnitude lower than that in acidic media.[34–36] Although the basic reaction mechanism of the alkaline HER has been verified to a certain extent, there are still many controversies in the research of its kinetics and energetics, and scholars in the fields of computational chemistry and electrochemistry have not yet reached a consensus. This situation has inspired researchers' strong interest in exploring the underlying reasons from multiple perspectives.[37–40] For example,
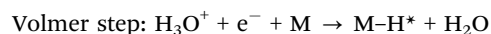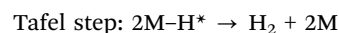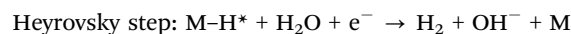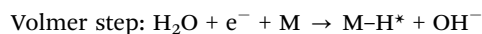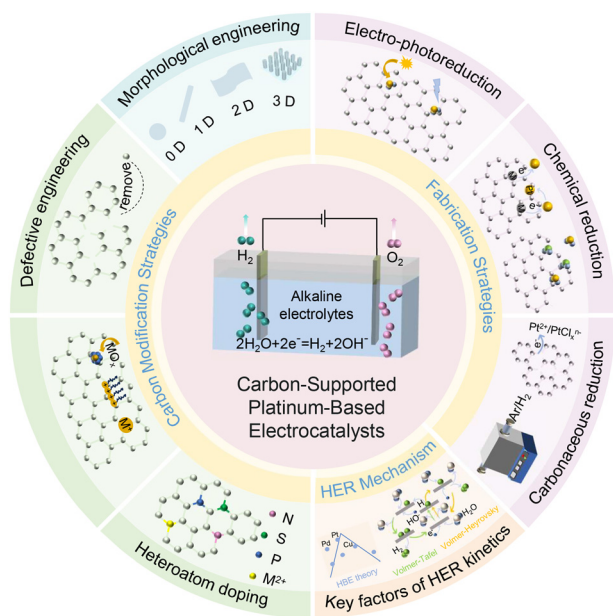

Fig. 1 Schematic diagram of the principal guidelines and performance improvement strategies for carbon-support Pt-based electrocatalysts for the alkaline HER.

Yan *et al.* conducted tests on polycrystalline Pt in electrolytes with different pH values (ranging from 0 to 13), deeply investigating the correlation between the hydrogen oxidation/evolution activity and the experimentally measured HBE.[41] Their research uncovers that HBE which varies with pH is the fundamental reason for the pH-dependent kinetics. More precisely, acidic conditions are marked by an elevated concentration of H^+ ions. These H^+ ions can rapidly adsorb onto the surface of Pt, facilitating the HER Volmer step. Therefore, HBE is regarded as a key descriptor for the HER. Wei *et al.* briefly summarized the slow reaction rate of the HER under alkaline conditions from the aspects of the barriers of water dissociation and the pH dependence of HBE, providing theoretical directions for engineering electrocatalysts to boost the efficiency of the alkaline HER activity.[31] Moreover, Zheng *et al.* conducted an in-depth analysis of the alkaline HER from multiple dimensions, such as the energetics and kinetics of the hydrogenation reaction on the metal surface and the controversy over activity descriptors.[42] As characterization techniques and computational chemistry continue to evolve, Qiao *et al.* revisited and systematically re-evaluated three prominent theories: the water dissociation theory, the HBE theory, and the interfacial water and/or anion transfer theory.[43] This conclusion has also been confirmed by the research of Menezes *et al.*[44] Similarly, Sun *et al.* systematically and thoroughly summarized the vital elements influencing the observable HER kinetics under alkaline conditions, covering the HBE theory, the role of OH*, the interfacial water, and the influence of alkali metal cations (AM^+).[45] Drawing on the extensive research achievements outlined above, we offer a comprehensive overview of the current key influencing factors and present our distinctive perspectives.

The water dissociation theory reveals the key regulatory role of the pH environment in HER kinetics.[14] Under acidic conditions, high concentration H^+ directly participates in the initial Volmer step as reactants. The sufficient supply of H^+ significantly reduces the activation energy of the Volmer reaction, enabling efficient generation of H* intermediates on the catalyst surface and accelerating subsequent Heyrovsky or Tafel reactions for high-efficiency hydrogen production. In stark contrast, alkaline media lack a high concentration of free H^+, and the generation of H* originates from water dissociation steps, forcing the HER process to overcome a higher energy barrier.[46] The hydroxide binding energy (OHBE), defined as the binding energy between the catalyst and OH^- intermediates, directly influences the difficulty of water dissociation. Excessively strong OHBE leads to over-adsorption of OH^- at active sites, blocking the generation pathway of H*; whereas insufficiently weak OHBE fails to effectively promote water dissociation, resulting in inadequate proton supply.[42] Therefore, under alkaline conditions, the accumulation of OH^- concentration on the catalyst surface forms a localized high OH^- environment, which thermodynamically and kinetically inhibits the water dissociation process. The competitive adsorption between OH* and H* on active sites reduces the number of H* adsorption sites and alters the electronic structure of active sites, further hindering the reaction progress.[39] Furthermore, OH* and H* exhibit strong competitive adsorption on the limited active sites of the catalyst. On one hand, this competition reduces the number of active sites available for H adsorption and reaction. On the other hand, adsorbed OH* may alter the electronic structure or steric hindrance of active sites, indirectly weakening the adsorption strength of H* or hindering subsequent Heyrovsky or Tafel steps.[40] This view has been verified by constructing Pt (111) catalysts with additional water dissociation sites (such as ($M(OH)_2$ clusters, where M = Fe, Co, Ni)).[47]

The HBE theory provides a critical theoretical interpretation of the HER mechanism from a kinetic perspective.[9] Ideal HER catalytic materials need to tune their binding energy with H* to an optimal range–an excessive HBE will significantly raise the activation energy barrier of the reaction, especially in high-pH systems, where this effect triggers a drastic decrease in the HER rate and exerts a remarkable inhibitory effect on catalytic efficiency.[48] At the essence of catalysis, an excessive HBE leads to hindrance in the desorption process of H* from the catalyst surface, significantly increasing the energy barrier of the rate-determining step. In an alkaline environment, the competitive adsorption of OH^- on the catalyst active sites and the change in proton supply pathway further amplify the negative impact of excessive HBE on reaction kinetics, resulting in a non-linear decay trend of catalytic efficiency.[49] This theoretical framework provides a clear thermodynamic-kinetic optimization direction for the design of efficient HER catalysts under high-pH conditions. The effect of interfacial water plays an indispensable role in the HER kinetics. The configuration of interfacial water is deeply intertwined with the pH-dependent changes in HER activity.[43] As the pH value gradually increases, the kinetic process of alkaline HER and the hydrogen generation rate show a decreasing trend, the charge transfer resistance correspondingly increases, and the adsorption rate of hydrogen ions also slows down accordingly. From a theoretical mechanism perspective, the correlation between the electrode potential and the potential of zero free charge (PZFC) has a significant impact on the reorganization energy of interfacial water molecules, thereby exerting a regulatory effect on the hydrogen adsorption process and reaction activity through this mechanism.[41] As a key descriptor of activity, the structure of the interfacial water will change with the variations in water concentration, the type of supporting salt, and the pH value. Specifically, different water concentrations and supporting salts affect the reduction activity of water. Typically, organic solvents are added or supporting salts are regulated to alter the water concentration. At higher water concentrations, water–water interactions are enhanced, and the formed water nanodomains promote the reaction through the Grotthuss diffusion mechanism, corresponding to higher HER activity.[44] Additionally, as the pH increases, the first layer of interfacial water transitions from a proton acceptor to a donor, while the activation energy for water dissociation changes in a specific order. The AM^+ theory further expands our understanding of the HER kinetics.[45] On the one hand, the complex of hydroxyl-water-alkali metal cations adsorbed on the surface of the catalyst can promote the transfer process of OH*, and AM^+ itself can also significantly change the transfer kinetics of OH*, thus having an important impact on the HER under alkaline conditions. On the other hand, the interaction between the metal cations and

the interfacial water will change the architecture of the interfacial water, and further affect the HER rate. It merits attention that as a result of the concentration distribution of OH* and AM$^+$ is closely related to the pH value, the pH environment on the surface of the catalyst becomes a key factor in controlling the HER kinetics.[50]

Although there are multiple explanations for the sluggish alkaline HER kinetics, controversies still exist in the related theoretical research, with a unified system and universal model yet to be established. Future research should focus on three primary aspects: (1) optimizing catalyst design by deepening the understanding of reaction mechanisms, which involves regulating metal cation-related factors, optimizing catalyst–intermediate interactions, reducing water dissociation energy barriers, and enhancing reaction rates; (2) combining multidisciplinary methods through the integration of experimental and theoretical approaches, specifically using *in situ* characterization techniques and density functional theory (DFT) calculations to investigate intermediate adsorption and charge transfer mechanisms, thereby providing theoretical support for catalyst design; (3) exploring new materials such as transition–metal-based composites and metal–organic frameworks (MOFs) to improve alkaline HER kinetics. Notably, carbon materials have demonstrated exceptional potential in alkaline water electrolysis, where carbon modification synergistically optimizes the kinetics of the HER through multi-dimensional regulation.[8–12] At the morphological regulation level, nanostructures such as carbon nanosheets and porous networks increase the exposure of active sites, control the size and dispersion of Pt particles, and shorten the ion diffusion path by optimizing the spatial topology. This synergizes with the pore structure to enhance the accessibility of active sites. In defect engineering optimization, defect sites on the carbon support anchor Pt particles to inhibit agglomeration while inducing interfacial charge polarization, reducing the energy barrier for water dissociation and enhancing the intrinsic catalytic activity. For electronic structure regulation, heteroatom doping (*e.g.*, N, S) leverages electronegativity differences to reconstruct the electron cloud on the carbon surface, optimizing the ΔG_{H^*} of Pt active sites *via* SMSI and accelerating the Volmer step kinetics. In terms of surface wettability regulation, hydrophilic/hydrophobic modifications optimize the contact efficiency of the three-phase interface (solid–liquid–gas), where hydrophobicity promotes H_2 bubble detachment and hydrophilicity enhances electrolyte penetration. For interfacial synergistic catalysis, the electronic coupling between the carbon support and Pt forms bifunctional catalytic sites that cooperatively promote water dissociation and hydrogen recombination, enhancing stability. As summarized in Table 1, carbon-supported Pt-based HER electrocatalysts exhibit competitive overpotentials at 10 mA cm^{-2}, favorable Tafel slopes, and enhanced stability in alkaline electrolytes. The following sections will systematically elaborate on recent advancements in carbon-supported Pt-based materials in alkaline HER systems.

3. Carbon modification strategies of carbon-supported platinum-based electrocatalysts for the alkaline HER

Sp^2-hybridized carbon, with remarkable advantages such as an ultra-high specific surface area, excellent electrical conductivity, and flexibility thermal elasticity, enables carbon-based materials

Table 1 Summary of the carbon-supported platinum-based electrocatalysts for the alkaline HER

Catalyst	Pt loading	η_{10} (mV)	Tafel slope (mV dec^{-1})	Mass activity (V *vs.* RHE)	Stability	Ref.
Pt/G–CNFs	3.4 µg cm^{-2}	177	72	0.626 A mg$_{Pt}^{-1}$ at −0.1 V	90 h at 10 mA cm^{-2}	58
NiPt–NC	0.27 mg cm^{-2}	48	50.3	0.67 A mg$_{Pt}^{-1}$ at −0.02 mV	30 h at 1.56 V	59
Ru–PtFeNiCuW/CNTs	7.67 wt%	16	27.9	—	50 h at 10 mA cm^{-2}	61
Pt/VGAr-5	0.71 µg cm^{-2}	124	36	44.8 A mg$_{Pt}^{-1}$ at −0.2 V	Over 24 h at 100 mA cm^{-2}	63
Pt–Ni$_4$Mo/CNT	0.14 mg cm^{-2}	18.6	37.4	6.97 A mg$_{Pt}^{-1}$ at −0.07 V	200 h at 100 mA cm^{-2}	67
Ru$_1$Pt$_2$@rGO	10.81 wt%	9	20.9	2.67 A mg$_{metal}^{-1}$ at −0.05 V	3000 cycles	69
Pt–NiO$_x$–H$_2$/C	50 µg cm^{-2}	39.6	24.49	6.07 A mg$_{Pt}^{-1}$ at −0.1 V	25 h at 10 mA cm^{-2}	81
Pt/8-NCNT	0.14 mg cm^{-2}	17	33.3	3.13 A mg$_{Pt}^{-1}$ at −0.1 V	100 h at 500 mA cm^{-2}	82
(Ru–P)#Pt/C	0.76 wt%	17	27	—	24 h at 10 mA cm^{-2}	86
P–Pt$_1$Ni$_2$NH/NGA	9.1 µg cm^{-2}	15	37	13.4 A mg$_{Pt}^{-1}$ at −0.1 V	20 h at 10 mA cm^{-2}	90
Pt-30/NCM	3.39 wt%	19.5	40.8	1.91 A mg$_{Pt}^{-1}$ at −0.05 V	3000 cycles	91
Pt/NSC	7.677 wt%	17.8	30.59	4.90 A mg$_{Pt}^{-1}$ at −0.1 V	50 h at 50 mA cm^{-2}	93
PtMo–NC	13.52 wt%	35	32	3.68 A mg$_{Pt}^{-1}$ at −0.05 V	5000 cycles	109
Pt/Ce–N–C	32 µg cm^{-2}	22	33.8	7.16 A mg$_{Pt}^{-1}$ at −0.05 V	200 h at 100 mA cm^{-2}	110
Pt$_5$/HMCS	7.6 µg cm^{-2}	46.2	48.1	3.23 A mg$_{Pt}^{-1}$ at −0.07 V	3000 cycles	112
Pt@CoN$_4$–G	12 µg cm^{-2}	39	29	1.15 A mg$_{Pt}^{-1}$ at −0.05 V	10 000 cycles	113
Pt–AC/Cr–N–C	1.72 wt%	19	30	7.9 A mg$_{Pt}^{-1}$ at −0.05 V	24 h at 10 mA cm^{-2}	114
Pt/TC2	—	58	65.5	1.115 A mg$_{Pt}^{-1}$ at −0.05 V	10 h at 10 mA cm^{-2}	118
Pt/C$_{60}$-2	0.053 mg cm^{-2}	25	55	—	100 h at 10 mA cm^{-2}	119
c-PRPDWNT/C	0.1 mg cm^{-2}	10	30.8	47.8 A g$_{metal}^{-1}$ at −0.02 V	100 h at 50 mA cm^{-2}	120
Pt$_3$Co@NCNT	0.4 mg cm^{-2}	36	34.8	—	100 h at 100 mA cm^{-2}	123
Co$_n$–Pt$_1$@NPC	6.47 wt%	20	29.07	1.36 A mg$_{Pt}^{-1}$ at −0.05 V	100 h at 10 mA cm^{-2}	124
PtC$_{60}$	0.4 mg cm^{-2}	24.3	30	1.55 A mg$_{Pt}^{-1}$ at −0.1 V	50 h at 10 mA cm^{-2}	125
PtRu/CNT@MO$_{2−x}$	4.6 µg cm^{-2}	53	48	12.3 A mg$_{metal}^{-1}$ at −0.07 V	2000 cycles	130
Pt–Co$_2$P/CC	3.33 wt%	2	44	—	200 h at 100 mA cm^{-2}	131
Pt@DG	1.57 wt%	37	53	26.05 A g$_{Pt}^{-1}$ at −0.1 V	5000 cycles	132

to serve as highly promising carriers for Pt-based electrocatalysts in the alkaline HER. Nonetheless, it is limited by easy corrosion in alkaline media, whose mechanism has been detailed in the introduction and will not be repeated here. There are multiple dimensions to enhance the kinetics of alkaline HER and catalytic material resilience: (1) interfacial charge transfer dynamics (conductivity optimization); (2) electronic structure modulation of active sites; (3) nanoconfinement effects on catalyst dimensions; (4) catalysts structural stability; (5) hydrophilic/hydrophobic balance regulation; (6) multi-mechanism synergistic effect. To further boost the performance of Pt-based catalysts, a suite of advanced carbon substrate engineering strategies have been implemented purposefully, covering two major aspects of morphological engineering and surface engineering (defect engineering, surface functionalization, and heteroatom doping), aiming to enhance the activity and stability of the alkaline HER from the above-mentioned effect directions. Next, we will discuss the structural modification strategies of carbon supports in detail.

3.1. Morphological engineering

The morphology of carbon supports significantly influences the activity, stability, and selectivity of electrocatalysts through multiple mechanisms:[51–54] (1) directly determining the available surface area and density of exposed active sites; (2) modulating electron transfer efficiency across the catalyst surface; (3) governing the structural integrity and long-term stability of the electrocatalyst system; (4) enabling precise spatial control over the distribution and accessibility of catalytic active centers. Carbon supports are typically classified by dimensionality into zero-dimensional (0D, e.g., diamond, carbon quantum dots, fullerenes), one-dimensional (1D, e.g., carbon nanotubes), two-dimensional (2D, e.g., graphene), and three-dimensional (3D, e.g., mesoporous carbon, carbon aerogel) architectures. In recent studies, through rational design and structural optimization of support architectures, the charge/mass transport kinetics and interfacial robustness of electrocatalysts can be substantially enhanced, consequently advancing their practical deployment in energy conversion systems and accelerating the development of sustainable energy conversion technologies.

0D carbon nanomaterials have garnered significant research interest owing to their tunable electronic structures, superior electrical conductivity, and exceptional chemical stability, as evidenced by recent breakthroughs in alkaline HER electrocatalysis.[55,56]

For instance, Dang et al. synthesized CDs/Pt-PANI catalysts by leveraging the strong bonding between the surface functional groups of carbon dots (CDs) and polyaniline nanosheets (PANI), which is confirmed by Fig. 2a.[57] Thanks to the synergistic effect of CDs, Pt, and PANI, these catalysts manifest superior efficiency: only 56 mV is needed to reach 10 mA cm^{-2} in 1 M KOH, outperforming 20 wt% Pt/C which requires 86 mV at an identical current density. To further investigate the influence of CDs on catalysts, Wang et al. proposed a heterostructure composed of graphene–carbon nanofibers (G–CNF) loaded with Pt nanoclusters and studied the effects of different contents of Pt nanoclusters and CDs on the HER performance.[58] Using a mixture of calcium lignosulfonate (LS) and CDs as the precursor, they

formed G–CNF through electrospinning and subsequent carbonization. As shown in Fig. 2b, the conductivity of the prepared G/CNFs gradually improved with the increase of the added CD content, which contributed to the enhancement of the alkaline HER activity. In addition to regulating the HER activity by optimizing the electron transport performance, CDs can also use surface defect sites as anchoring sites to load Pt NPs. By triggering the SMSI effect, the intrinsic activity and structural stability of the catalyst are synergistically improved. This strategy regulates the electron coupling between the support and metal active sites through defect engineering, which can not only promote the adsorption–desorption kinetics of reaction intermediates but also inhibit the agglomeration and sintering of Pt particles through interfacial electron reconstruction, realizing the dual optimization of catalytic performance. Liu et al. anchored Pt on Ni and N co-doped CDs (Ni–NC) with rich defect structures and atomically dispersed Ni–N$_5$ sites to prepare NiPt–NC electrocatalysts with high dispersion and low Pt loading.[59] Fig. 2c revealed that the interaction between Pt NPs and the surrounding Ni–N$_5$ sites led to electron enrichment around Pt, optimizing the desorption of OH* and the adsorption/dissociation of H$_2$O (volmer step), enhancing the intrinsic activity of Pt for the alkaline HER, with a 48 mV overpotential at 10 mA cm^{-2}. These studies provide constructive guidance for the subsequent study of 0D carbon materials as supports.

Carbon nanotubes (CNTs) and carbon nanofibers (CNFs), as prototypical 1D carbon nanomaterials, have garnered significant attention in alkaline HER electrocatalysis owing to their exceptional electrical conductivity, superior mechanical robustness, remarkable chemical stability, and tunable electronic structures.[65,66] For instance, Zhang et al. prepared a series of surfactant-free noble metal doped Ru/CNT (M–Ru/CNT, M = Pt, Rh, Pd, Ir, CNT stands for carbon nanotube) by microwave reduction method, using CNTs with large specific surface areas, strong conductivities and high mechanical strengths as the carrier to make the active ingredients highly uniformly dispersed and increase the number of active sites.[60] DFT demonstrates that Pt–Ru/CNT can significantly optimize ΔG_{H*} and accelerate the release of H$_2$ (Fig. 2e), thereby promoting alkaline HER kinetics, requiring only 4 mV overpotential to drive 10 mA cm^{-2} in 1.0 M KOH (Fig. 2d). Liu et al. prepared small-sized (3–4 nm) M–Ni$_4$Mo NPs (M = Pt, Ru, Pd) supported on CNT via a simple, rapid, and solvent-free microwave reduction method.[67] The Pt–Ni$_4$Mo/CNT catalyst with optimal atomic ratio and loading exhibits exceptional HER performance in 1 M KOH electrolyte, achieving an overpotential of 18.6 mV at 10 mA cm^{-2}. Benefiting from the SMSI effect, the catalyst also demonstrates excellent long-term stability, maintaining catalytic activity without significant decay after continuous operation at a high current density of 100 mA cm^{-2} for 200 hours. This performance advantage stems from the synergistic regulation of the interfacial electronic structure of the catalyst. On one hand, the electronic coupling between the Ni$_4$Mo alloy and the CNT support optimizes the hydrogen adsorption energy barrier; on the other hand, the SMSI induced interfacial charge reconstruction effectively inhibits the agglomeration and sintering of Pt active sites, achieving a dual
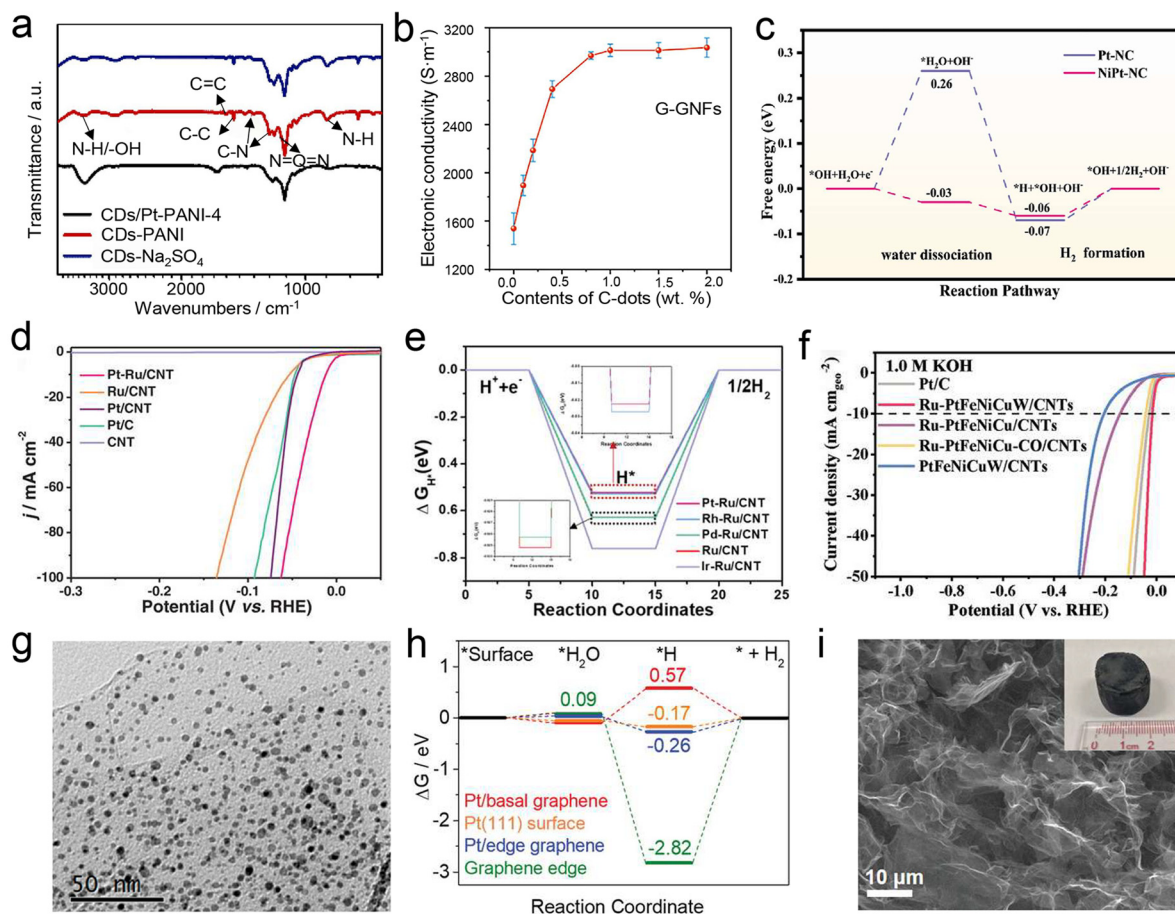
Fig. 2 (a) FTIR spectra of CDs/Pt-PANI-4, CDs-PANI, and PANI-Na$_2$SO$_4$. Reproduced with permission.[57] Copyright 2019, Elsevier. (b) Electronic conductivity curves of G−CNFs with different contents of CDs. The pyrolysis temperature is 1400 °C. Reproduced with permission.[58] Copyright 2022, Wiley-VCH GmbH. (c) Free energy diagrams of the elementary steps in the HER. Reproduced with permission.[59] Copyright 2025, Elsevier. (d) HER polarization curves of CNT, Pt/C, and M−Ru/CNT (M = Rh, Pd, Ir) catalysts in N$_2$-saturated 1.0 M KOH solution. (e) ΔG_{H*} of Pt−Ru/CNT, Rh−Ru/CNT, Pd−Ru/CNT, Ir−Ru/CNT, and Ru/CNT. Reproduced with permission.[60] Copyright 2021, Wiley-VCH GmbH. (f) HER performance in 1.0 M KOH electrolytes. Reproduced with permission.[61] Copyright 2024, Wiley-VCH GmbH. (g) TEM image of Pt$_3$Co/NG-700 catalyst. Reproduced with permission.[62] Copyright 2020, American Chemical Society. (h) Calculated Gibbs free energy of the alkaline HER reaction pathway on Pt/graphene edge, Pt/basal graphene, Pt (111) surface, and a zigzag graphene edge. Reproduced with permission.[63] Copyright 2022, Wiley-VCH GmbH. (i) SEM image of 3D porous WGA. Inset: Optical picture of WGA. Reproduced with permission.[64] Copyright 2021, Wiley-VCH GmbH.

improvement in catalytic activity and structural stability. Moreover, Wang et al. prepared Ru-doped PtFeNiCuW octahedral high-entropy alloy (HEA) nanocrystals on CNTs (Ru–PtFeNi-CuW/CNT).[61] High-angle annular dark field-scanning transmission electron microscopy (HAADF-STEM) images demonstrate that the HEA octahedrons are homogeneously distributed on the CNTs. Fig. 2f reveals that the catalyst exhibits a low overpotential of 16 mV in an alkaline electrolyte (at a current density of 10 mA cm^{-2}). In a two-electrode alkaline system, it can operate stably for 1200 h at a current density of 50 mA cm^{-2}. The above work demonstrates that CNTs, with their large specific surface area and excellent stability, serve as superior supports for loading Pt, holding profound significance for advancing the commercial application of carbon-supported Pt-based catalysts.

Graphene, a representative 2D carbon-based material, boasts unique structural advantages such as a large surface area, high electrical conductivity, and good chemical stability.

These properties endow graphene-based electrocatalysts with enhanced alkaline HER performance.[68] Lin et al. anchored Pt$_3$Co NPs onto nitrogen-doped graphene (NG) (Pt$_3$Co/NG-700) through a simple pyrolysis method.[62] The SMSI between NG and Pt$_3$Co led to the formation of small-sized and ordered Pt$_3$Co NPs during the high-temperature treatment, as demonstrated in Fig. 2g. Owing to the synergistic coupling effect between the ordered Pt$_3$Co nanocrystals and the NG support, the mass activity of Pt$_3$Co/NG-700 reaches 51.8 times compared with the commercial Pt/C. This synthesis strategy regulates the growth kinetics of NPs through the SMSI effect, not only achieving high-density uniform distribution of active sites but also optimizing the hydrogen adsorption energy barrier through the electronic coupling between the support and the metal, providing new ideas for the design of efficient electrocatalytic systems. Tsounis et al. utilized the enhanced reactivity of graphene edges to anchor ultra-low mass-loaded Pt SACs

onto the edges of edge-rich, vertically oriented graphene.[63] This enhanced reactivity enables the anchoring and tuning of the electronic states of SACs. Specifically, the edge-anchored Pt SACs have a firm coupling with the π electrons of graphene. This interaction results in a higher occupancy of the Pt 5d orbitals, shifting the d-band center towards the Fermi level, thus improving the adsorption of H* in the HER (Fig. 2h). To arrive 10 mA cm^{-2}, 1 μg Pt/C and Pt/VG Ar-5 requires overpotentials of 199 mV and 124 mV, respectively. Besides, Yang *et al.* prepared Ru–Pt heterogeneous bimetallic NPs (Ru$_x$Pt$_y$@rGO) on reduced graphene oxide (rGO) *via* a simple "simultaneous reduction" hydrothermal method, simplifying the catalyst synthesis process.[69] The rGO as a support can significantly enhance the catalyst's electrical conductivity. Ru$_1$Pt$_2$@rGO with the optimal Ru/Pt ratio exhibits a faster Volmer–Tafel mechanism in 1 M KOH solution, with an overpotential of 9 mV at a current density of 10 mA cm^{-2}, outperforming other Ru-based or Pt-based monometallic catalysts reported in the literature. In the future, graphene is expected to leverage its unique structure to innovate carbon-supported Pt-based catalysts by optimizing electron conduction and enhancing interfacial stability.

Compared with low-dimensional carbon materials with a simple structure, 3D carbon materials have a complex structure and possess significant advantages such as high mechanical strength, strong designability, and excellent environmental adaptability.[70–72] Li *et al.* electrochemically deposited Pt NPs on a tungsten oxide/reduced graphene oxide aerogel (WGA) support.[64] The WGA exhibits a typical 3D interconnected porous structure (Fig. 2i), featuring abundant oxygen vacancies and hierarchical pore sizes, which plays the role of anchoring Pt NPs, providing continuous mass transport and electron transfer channels, and regulating the electronic state of the Pt surface. Therefore, Pt/WGA exhibits high HER activity and durability, with an overpotential of 42 mV and 40 h chronopotentiometry at 10 mA cm^{-2}. Park *et al.* designed a new type of CNT-based electrode that can produce a 3D porous structure when the CNT array is cross-woven.[73] The 3D porous structure contains square pores that provide high conductivity and a large surface area, and the HER electrocatalyst can be dispersed in a hierarchical porous CNT framework, which is called the M_CNTs (M: HER catalyst) electrode. The CNT-based NiFeO$_x$ and Pt electrodes exhibited sustained performance without any performance loss during anion-exchange-membrane water electrolysis (AEMWE) operation for 40 h. 3D carbon materials show extremely broad application prospects in the field of carbon-supported Pt-based catalysts for alkaline HER, and their unique structural advantages will continue to provide support for catalytic performance optimization. In terms of activity improvement, the large specific surface area of 3D carbon materials can significantly increase the loading sites of Pt, promote the uniform dispersion of Pt particles, reduce agglomeration, and thus increase the number of active sites of the catalyst. In terms of stability, 3D carbon materials have good mechanical and chemical stability, which can provide stable support for Pt in an alkaline environment, inhibit the dissolution and agglomeration of Pt during the reaction, and prolong the service life of the catalyst.

The morphological dimensions of carbon materials considerably impact catalyst performance. 0D carbon materials leverage quantum confinement effects and high surface activity; adjusting particle size and functional groups optimizes catalyst adsorption and dispersion. 1D carbon nanotubes, characterized by high aspect ratios, conductivity, and hollow structures, enhance catalyst loading *via* diameter control. 2D graphene utilizes its large surface area and stability, boosting catalyst anchoring through defect introduction. 3D carbon materials with porous architectures enable uniform catalyst dispersion and protection. Combining multi-dimensional carbon materials with precise control represents a critical future direction for catalyst performance improvement.

3.2. Surface engineering

Surface engineering of Pt-based electrocatalyst supports encompassing defect engineering, surface functionalization, and heteroatom doping. It is not only an effective way to stabilize and anchor co-catalysts but also a strategy to induce specific arrangements and combinations of co-catalysts.[74] Understanding and leveraging surface engineering is key to enhancing catalyst intrinsic activity and driving further research progress.

3.2.1. Defective engineering. Generally speaking, defects in carbon-based materials are categorized into intrinsic and non-intrinsic types.[75–77] Intrinsic defects stem from non-sp^2 hybridized carbon atoms, covering point, single vacancy, multiple vacancies, line, and non-plane carbon atom introduction defects. Non-intrinsic defects result from covalent bonding of non-carbon atoms to carbon atoms, including out-of-plane heteroatom introduction and in-plane heteroatom doping defects. The defect strategy enables firm anchoring of Pt species on defect-rich carbon supports, enhancing atom utilization and accelerating reaction kinetics.[75] For example, Chen *et al.* prepared defect-rich porous Co$_1$NC supports by using Co-doped zeolite imidazole framework-8 (ZIF-8) precursor, which has the characteristics of high specific surface area, multiple functional sites, and adjustable pore size, and then Pt$_1$/Co$_1$NC catalysts were fabricated by room temperature electroreduction.[78] Raman spectroscopy was used to characterize the degree of defects in Co$_1$NC and NC. As proved in Fig. 3a, Co$_1$NC ($I_D/I_G = 3.48$) has more defects than NC ($I_D/I_G = 2.90$). It is worth noting that when Co$_1$NC is loaded with Pt, the ratio of I_D/I_G decreases significantly, and compared with NC loaded with Pt, the ratio does not change much, proving that Co$_1$NC is used as a carrier, and more defects are used to anchor Pt single atoms (Fig. 3b). This strategy significantly improves the utilization rate of Pt atoms, enabling a current density of 10 mA cm^{-2} to be achieved with a driving potential of only 22.85 mV. To further investigate the influence of defects on Pt loading, Cheng *et al.* reported a novel one-step carbon defect-driven chemical deposition method for the preparation of ultra-small but well-defined and stable Pt single atom clusters (Pt–AC/DG) supported by graphene (DG) structures with different defect densities.[79] With the increase of NH$_3$ etching time, the nitrogen doping level rises. Concurrently, both the I_D/I_G value and the defect density increase (Fig. 3c and d). The resulting Pt–AC/DG-500 catalyst has low overpotential ($\eta_{10} = 21$ mV) and high HER mass activity, with excellent stability, thus improving Pt

utilization. Skillful application of defect engineering strategies can modulate catalyst intrinsic activity, and enhance atomic utilization and catalyst stability, guiding further exploration of defect strategies' significance in nanomaterial design.

3.2.2. Surface functionalization. Surface functionalization refers to the introduction or modification of specific chemical groups or nanostructures on the surface of a material to change its physicochemical properties and surface performance. Functional groups introduced into the carbon matrix (such as oxygen functional groups such as hydroxyl, epoxy, carboxyl, organometallic complexes, and metal cations) can change the electronic configuration of the carbon skeleton and provide a medium for interaction with other catalysts.[83,84] Typically, Ye *et al.* synthesized single Pt atoms anchored on aniline-stacked graphene (Pt SASs/AG) through a simple microwave reduction method.[80] Aniline molecules functionalize graphene *via* π–π interactions, making it hydrophilic and enabling uniform redispersion in an aqueous solution (Fig. 3e). As a result, the prepared Pt SASs/AG exhibits outstanding HER activity (η_{10} = 12 mV).

As expected, the increase in hydrophilicity of the carbon support surface contributes to the enhancement of HER activity. Additionally, metal oxides show strong potential in functionalizing

carbon supports, which can significantly enhance their interaction with Pt species. Sun's group reported a surface functionalization strategy to provide specific catalytic activity and enhance the interaction with metal species by modifying transition metal oxide clusters on commercial carbon black.[81] Specifically, NiO_x clusters were modified on commercial carbon black, and then Pt clusters were synthesized by the alkali-ethylene glycol method and anchored on the functionalized carbon black surface. As verified in Fig. 3f, Pt–NiO_x/C exhibited higher white line intensity than Pt/C, indicating that the interaction at the heterostructure interface contributes to the increase in the average oxidation state of Pt. The Ni K-edge X-ray Absorption Near-Edge Structure (XANES) spectrum confirmed that the valence state of Ni was reduced due to the transfer of electrons from Pt clusters to NiO clusters at the heterostructure interface. In the case of NiO_x clusters decorated with carbon black, a strongly coupled cluster–cluster heterostructure (Pt–NiO_x/C) consisting of Pt clusters and NiO_x clusters is formed, which can greatly enhance the evolution kinetics of alkaline hydrogen, achieving 39.6 mV at 10 mA cm^{-2}, while Pt/C requires 131 mV (Fig. 3g). Furthermore, the synergistic effect of different functional groups with Pt has been demonstrated to accelerate the HER reaction kinetics. For instance, Yu *et al.*
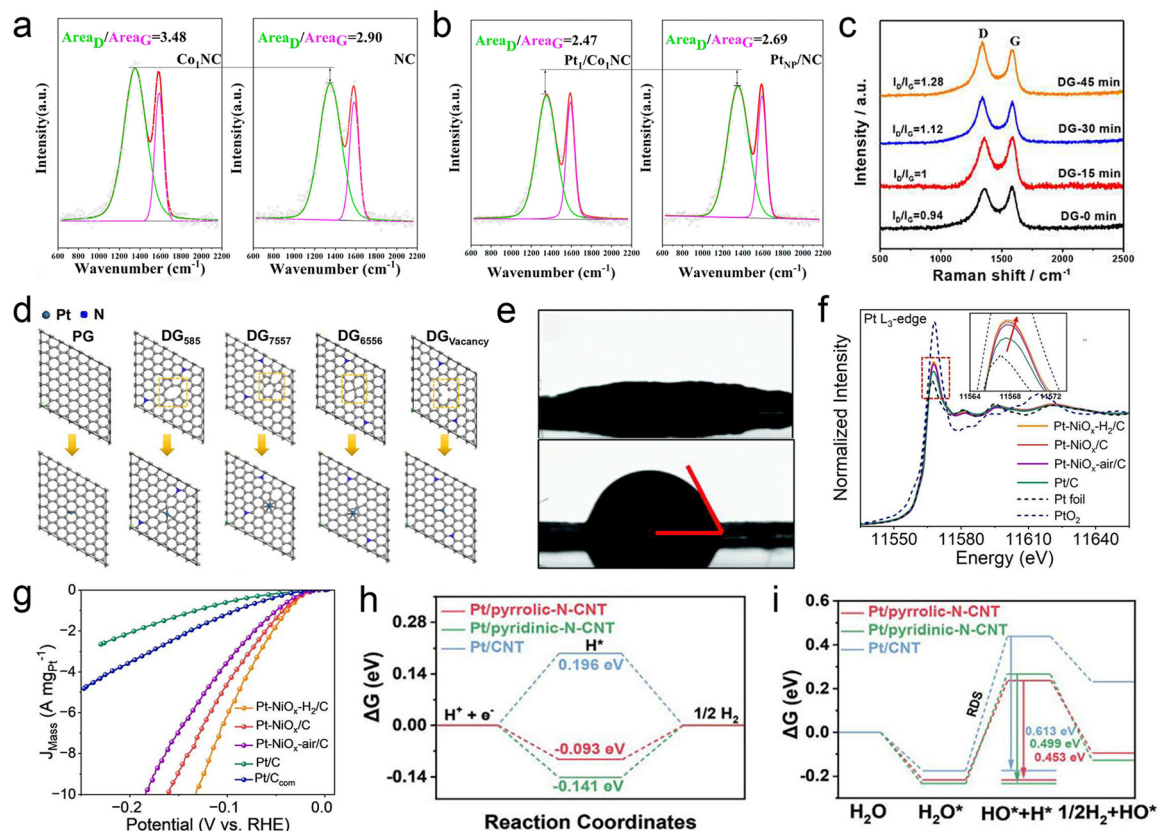
Fig. 3 (a) Raman spectra of Co_1NC and NC. (b) Raman spectra of Pt_1/Co_1NC and PtNP/NC. Reproduced with permission.[78] Copyright 2022, Elsevier. (c) The corresponding Raman spectra of NG after N removal (*i.e.*, DG). (d) DFT calculations with the models of PG, DG_{585}, DG_{7557}, DG_{5665}, and $DG_{vacancy}$. Reproduced with permission.[79] Copyright 2020, American Chemical Society. (e) Water contact angles of (up) Pt SASs/AG and (down) Pt/C. Reproduced with permission.[80] Copyright 2019, The Royal Society of Chemistry. (f) Pt L_3-edge EXAFS spectra (inset: the magnified pre-edge XANES region). (g) Mass activity of catalysts in 1.0 M KOH solution. Reproduced with permission.[81] Copyright 2025, Wiley-VCH GmbH. (h) The adsorption free energies of H*. (i) The free energy profiles for the HER in an alkaline medium from H_2O to H_2. Reproduced with permission.[82] Copyright 2022, Wiley-VCH GmbH.

integrated the advantages of Pt-based catalysts and nitrogen-doped carbon materials, and designed a series of Pt/X-NCNT (X = 4, 8, 12, 16) catalysts by virtue of the SMSI effect.[82] DFT calculations demonstrate that the Pt surface with pyridinic-N and pyrrolic-N functional groups exhibits a slightly negative ΔG_{H^*}, which is much lower than that of Pt/CNT (Fig. 3h), revealing the electronic coupling between Pt active sites and nitrogen functional groups. The HER free energy curve from H_2O to H_2 in the alkaline medium can be seen in Fig. 3i, further proving the fast HER kinetics, with an overpotential of 17 mV at 10 mA cm^{-2}. This provides a new paradigm for constructing electrocatalytic systems with both high activity and stability through the synergistic regulation of functional groups and metal active centers. The above works reveal that functionalization of carbon surfaces can enhance the performance of catalysts in alkaline HER by strengthening their interaction with Pt and optimizing the interface.

In conclusion, surface functionalization is an efficient strategy for modifying carbon supports. It can notably improve the hydrophilicity of carbon supports, enabling their uniform dispersion in aqueous solutions and facilitating the loading and dispersion of active components. Moreover, surface modification can regulate properties such as the electronic structure and defect density of carbon supports, enhancing the interaction with active components and thus optimizing the activity, stability, and selectivity of catalysts.

3.2.3. Heteroatom doping. Heteroatom doping serves as a versatile approach for precisely tailoring the electronic configuration and electrochemical performance of carbon-based materials. The strategic incorporation of heteroatoms with distinct electronegativities (*e.g.*, N, P, S, O, B) into graphitic lattices induces significant electron density redistribution and promotes the generation of charged active sites in the catalyst (Fig. 4a).[85,86] Moreover, due to the difference in electronegativity and spin density, the charge density or spin density of carbon atoms in the lattice is usually changed by neighboring heteroatoms, thereby regulating the work function of the catalytic active center and promoting the adsorption of reactants.[87–89] Nitrogen has emerged as the most prevalent heteroatom dopant in carbon matrices due to its atomic radius being 5% smaller than carbon's (0.75 *vs.* 0.77 Å) and electronegativity 0.49 Pauling units higher (3.04 *vs.* 2.55).[55,90] The predominant types of doped nitrogen atoms encompass pyridinic nitrogen, pyrrolic nitrogen, graphitic nitrogen, and oxidized nitrogen. In general, the incorporation of heteroatoms with diverse structures into various positions is capable of exerting an impact on the catalytic efficiency or the selectivity of catalytic reactions.

For example, Tian *et al.* precisely controlled the dispersion and coordination of Pt on hierarchical nitrogen-doped carbon nanocages (hNCNCs) through thermally driven Pt migration.[91] The hNCNC support has a large specific surface area (620 m^2 g^{-1}), coexisting micro-meso-macroporous structures, a high N content (9.6 atomic percentage), and high intrinsic conductivity (1362 S m^{-1}), affecting the HER performance by influencing the Pt coordination environment. Due to differences in the coordination environment, Pt–N$_2$Cl$_2$ shows the optimal HER activity (6 mV at 10 mA cm^{-2}), while

Pt–N$_4$C$_{4-x}$ exhibits poor HER activity (321 mV at 10 mA cm^{-2}). Yang *et al.* constructed hierarchical porous phosphide Pt–Ni nano-hexa-pods/nitrogen-doped graphene aerogel (P–PtNiNH/NGA) through an oxidation–phosphatization controlled reconstruction strategy (Fig. 4b).[92] The hierarchical porous structure of NGA and its excellent anchoring effect on P–PtNiNH prevent the aggregation of Pt NPs and Ostwald ripening. As displayed in Fig. 4c, the dispersion of P–PtNiNH in NGA confirms this point. P–PtNiNH/NGA exhibits excellent alkaline HER activity and remarkable stability, with an ultra-low overpotential of 15 mV at a current density of 10 mA cm^{-2}. Li *et al.* uniformly anchored Pt nanoclusters (∼1.6 nm) onto an ordered macroporous nitrogen-doped carbon support (Pt-30/NCM) through the polystyrene sphere templating method followed by an impregnation method.[93] NCM features a uniform polyhedral nitrogen-doped carbon framework (∼675 nm) and an arrangement of interconnected ordered macropores (∼120 nm) (Fig. 4d), which can form channels for the rapid transport of electrons, ions, and molecules. Moreover, the DFT result in Fig. 4e confirms that the active Pt nanoclusters can interact with the nitrogen-doped carbon, inducing a favorable electron distribution, which is beneficial for the dissociation of water in an alkaline medium and the subsequent desorption of intermediate products (OH* and H*). Pt-30/NCM exhibits outstanding HER activity (η_{10} = 19.5 mV) in 1.0 M KOH, with only 5 mV attenuation at 10 mA cm^{-2} after 3000 cycles. In summary, N doping in carbon can regulate the electronic structure and surface properties of carbon supports, enhancing the anchoring effect on Pt species, inhibiting their agglomeration and dissolution, and promoting the dissociation kinetics of H_2O in alkaline HER. N doping also improves the electrical conductivity of carbon supports, synergistically enhancing the activity and stability of catalysts to achieve efficient catalysis under low Pt loading.

Sulfur (S) atoms are extensively utilized for doping carbon materials, leveraging their distinctive attributes: a large atomic radius, low electronegativity, abundant electrons, and the ability to form diverse covalent bonds. These characteristics could synergistically enhance the catalytic performance of resultant catalysts.[94–96] The electronegativity difference between S and carbon endows S doping with unique electron-regulating ability, which can significantly alter the surface electronic structure of carbon materials.[97] Additionally, S doping can enhance the SMSI between the support and metal, significantly accelerating charge transfer kinetics through interfacial electron reconstruction. This effect originates from the charge redistribution on the support surface induced by the electron-withdrawing property of S atoms: (1) optimizing the electron density of metal active sites; (2) shortening the charge migration path by enhancing interfacial coupling.[98,99] Yan *et al.* reported metal size-dependent charge transfer of Pt single atoms and nanocluster catalysts based on mesoporous S-doped carbon (S–C) (Fig. 4f). Specifically, the S–C support captures electrons from Pt single atoms through strong chemical Pt–S interactions. However, when the Pt size increases to nanoclusters, the direction of electron transfer reverses, with electrons flowing from S–C to Pt.[100] As a result, the PtSA/S–C catalyst with atomically dispersed Pt atoms exhibits
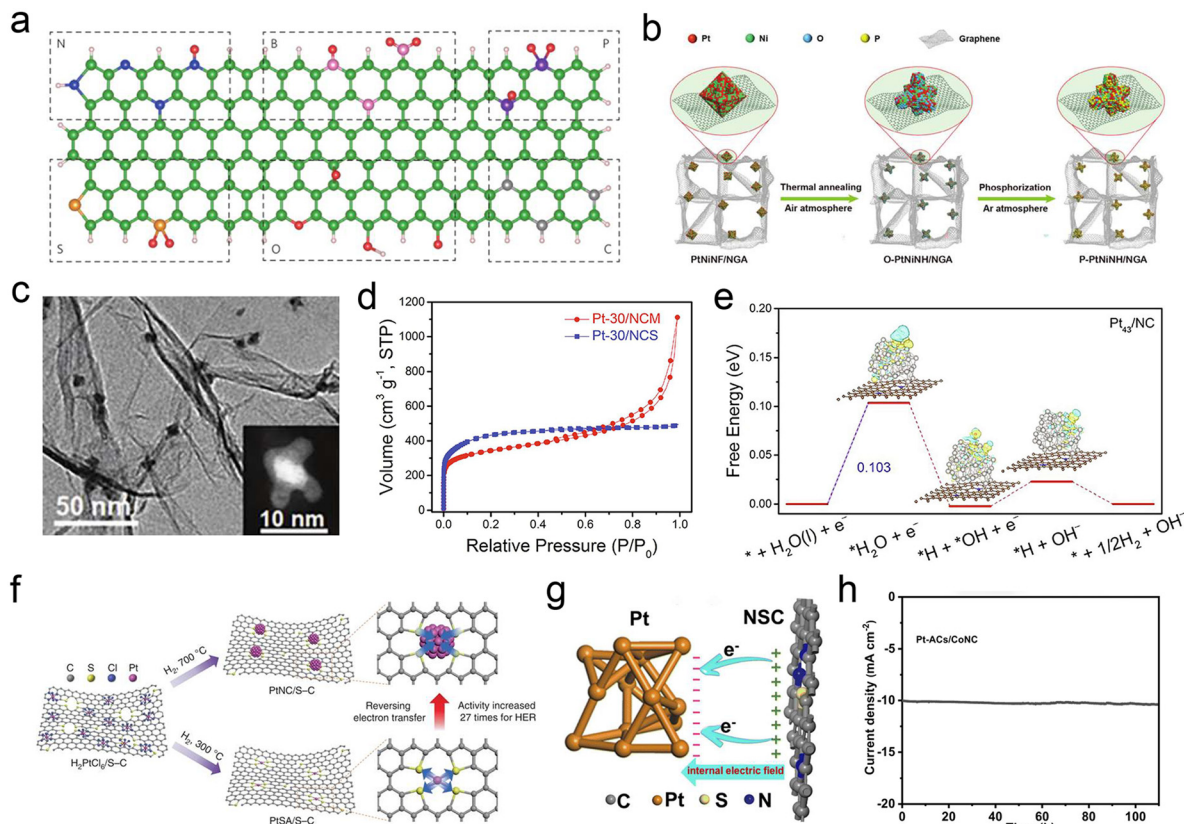
Fig. 4 (a) Schematic summary of the heteroatom doping configurations: (top row, from left to right) pr-N, py-N, g-N, N−O, B−2C−O, B−3C, B−C−2O, P−3C(−O) and P−2C(−2O); (bottom row, from left to right) th-S, S−2O, py-O, C−O−C, C−OH, C≡O, g-C, z-C and a-C. Green/grey, pink, blue, red, gold, purple, and white represent C, B, N, O, S, P, and H atoms, respectively. Reproduced with permission.[85] Copyright 2016, Nature. (b) Synthetic procedure for the P−PtNiNH/NGA. (c) TEM image of P-Pt₁Ni₂NH/NGA. Reproduced with permission.[92] Copyright 2024, Wiley-VCH GmbH. (d) N₂ adsorption−desorption isotherms for Pt-30/NCM and Pt-30/NCS. (e) Free energy diagram of alkaline HER on Pt₄₃/NC. Reproduced with permission.[93] Copyright 2022, Elsevier. (f) Schematic model of the catalyst preparation process and metal size-dependent charge transfer. PtSA/S−C and PtNC/S−C were prepared by wet impregnation of chloroplatinic acid on the S−C supports followed by H₂-reduction at 300 and 700 °C, respectively. When Pt size increases from single atom to nanocluster, the electron transfer direction is reversed, resulting in greatly enhanced activity for catalyzing HER. Reproduced with permission.[100] Copyright 2019, Nature. (g) Schematic illustration of the internal electric field between Pt and NSC. Reproduced with permission.[101] Copyright 2025, The Royal Society of Chemistry. (h) Chronoamperometry curve of Pt−ACs/CoNC obtained at the overpotential of 27 mV. Reproduced with permission.[102] Copyright 2022, Nature.

relatively poor HER activity, requiring an overpotential of 53 mV at 10 mA cm⁻². In contrast, the PtNC/S−C catalyst demonstrates significantly higher activity, achieving an ultra-low overpotential of only 11 mV at 10 mA cm⁻². Moreover, Li *et al.* innovatively proposed a S doping strategy to achieve the synergistic regulation of confined encapsulation of Pt NPs and SMSI by constructing a nitrogen−S co-doped carbon-based carrier (NSC).[101] On the one hand, the introduction of S atom doping provides more anchoring sites, enhances the coordination with the active component Pt, significantly improves Pt capture efficiency, and enables uniform deposition to form Pt NPs. On the other hand, the S atom doping activation strategy enhances the regulatory mechanism of the metal−support interaction and promotes charge redistribution at the interface simultaneously. This interfacial engineering not only precisely reconstructs the coordination microenvironment and electronic structure of Pt species but also constructs a directional charge transfer channel at the heterojunction interface (Fig. 4g), only requiring 17.8 mV to

reach 10 mA cm⁻² in 1.0 M KOH. Experimental results demonstrate that S-doped carbon materials can significantly enhance the SMSI between the support and metal components by regulating the surface electronic structure of carbon-based matrices, ultimately achieving leapfrog improvement in catalytic performance.

In addition to single-atom doping, many studies have shown that multi-atom doping can also enhance catalytic performance.[103–105] For example, Zhao *et al.* anchored Pt atomic clusters on isolated Co atoms and N co-doped porous carbon (Pt−ACs/CoNC).[102] The isolated CoN₄ species provided sufficient anchoring sites to stabilize the Pt clusters. The strong interaction between CoN₄ and Pt AC led to charge redistribution, realizing excellent stability (over 100 h of HER, Fig. 4h). Wang *et al.* proposed the synthesis of a Pt SA and NC coupled catalyst (Pt SAs−Pt NCs/NSC) anchored by N, S co-doped carbon (NSC) derived from coal pitch rich in vacancy defects by using the defect-induced electron redistribution effect.[106]

The co-doped S and N atoms in the carbon material can not only serve as anchoring sites to stabilize the Pt atoms but also regulate the electronic structure of the Pt atoms, promoting the HER process, and achieving an overpotential at 26 mV@10 mA cm^{-2}. Carbon doping with multiple atoms or co-doping can modulate the electronic structure of carbon supports through synergistic effects, enhance the interfacial interaction with Pt, improve the electrical conductivity, hydrophilicity and mechanical strength of supports, and optimize reaction kinetics and durability. This provides an important direction for designing highly active alkaline HER catalysts with low Pt loading. Heteroatom doping proves to be an exceptionally potent strategy for the modification of carbon materials. Through the meticulous adjustment of their electronic structure and the deliberate induction of vacancy defects, this method generates highly favorable sites that enable the robust and efficient anchoring of co-catalysts. Consequently, it greatly bolsters the overall catalytic performance, thereby presenting substantial potential for diverse catalytic applications.

To conclude, for carbon-supported Pt-based electrocatalysts, carbon materials suffer from corrosion in alkaline media due to electrochemical oxidation, nucleophilic attack of OH^{-}, galvanic corrosion, and dissolution–deposition effects. Therefore, a series of advanced carbon support engineering strategies, covering two major aspects of morphology engineering and surface engineering (defect engineering, surface functionalization, and heteroatom doping), have been applied to reduce carbon corrosion and further enhance the activity and stability of Pt-based catalysts. Next, we will elaborate on the fabrication strategies of carbon-supported Pt-based catalysts to further illustrate the interaction between carbon supports and Pt and the performance enhancement effects.

4. Fabrication strategies of carbon-supported platinum-based electrocatalysts for alkaline HER

Based on the systematic analysis of the advantages of carbon matrices as supports and their optimization strategies in the previous sections, this section focuses on the crucial role of Pt nanostructure engineering in carbon-supported Pt-based catalyst systems. The nanostructural characteristics of Pt, including size regulation, morphology design, and alloying strategies, all have a significant impact on the catalytic activity of the alkaline HER. The precise construction of Pt nanostructures highly depends on the selection and optimization of synthesis methods. In the preparation of Pt-based catalysts, reduction methods are commonly used to obtain active Pt species. The carbon support not only exhibits excellent reducibility but also provides an ideal platform for synthesis techniques such as electrodeposition due to its unique electrical conductivity. This dual characteristic enables a synergistic promotion effect between the carbon support and active Pt components during the synthesis process. Therefore, this section systematically reviews the mainstream synthesis techniques for carbon-supported Pt-based catalysts, which are classified into three major categories according to

their reaction mechanisms: (1) carbonaceous reduction (such as pyrolysis high temperature assisted reduction and carbon support intrinsic defect reduction), (2) chemical reduction encompassing displacement reactions and agent-assisted reduction, and (3) photoelectric reduction including electrochemical deposition and photoinduced reduction. Through a comparative analysis of different synthesis strategies, this review focuses on exploring their technical features in terms of nanoparticle size control, dispersion uniformity, and environmental friendliness, clarifies the advantages and limitations of each method, and provides a theoretical basis for the rational design of high-performance carbon-supported Pt-based HER catalysts.

4.1. Carbonaceous reduction method

The typical representative of the carbon reduction method is pyrolysis, which is a general method for synthesizing new materials or chemicals through high-temperature heat-driven chemical reactions.[107] It is widely used in the preparation of carbon-supported Pt-based catalysts, and the core advantage is that the resulting catalyst has excellent structural stability.[91,108–110] The process can be achieved in a variety of atmospheres (such as Ar, N$_2$, H$_2$/N$_2$), in which the highly dispersed metal atoms, particles, clusters, or alloys are generated through the controlled decomposition of metal precursors.[111]

Lou's group reported the synthesis of Pt$_5$/HMCS electrocatalyst via pyrolysis of a prefabricated Pt$_5$(GS)$_{10}$/HMCS (GS = deprotonated glutathione, HMCS = hollow mesoporous carbon spheres) composite in an Ar/H$_2$ (95/5) atmosphere, which was prepared by sonicating Pt$_5$(GS)$_{10}$ clusters with HMCS in aqueous suspension at ambient temperature, followed by centrifugal collection and vacuum drying (Fig. 5a).[112] During the annealing process, the GS ligands were removed, and the Pt clusters were confined in the pore channels of HMCS, maximizing the use of precious Pt atoms. As shown in Fig. 5b, the Pt atoms are evenly distributed on the porous carbon support, and the catalyst exhibits excellent alkaline HER activity, requiring 46.2 mV overpotential at a current density of 10 mA cm^{-2} (Fig. 5c). However, the stability of this catalyst in long-term alkaline electrolysis still requires systematic verification. Among them, whether the Pt clusters confined in the pores of HMCS will undergo agglomeration and dissolution due to the dissolution–deposition process caused by electrochemical corrosion or the size evolution of nanoclusters due to Ostwald ripening has not been sufficiently supported by experimental evidence. What is more, Zhang et $al.$ used g-C$_3$N$_4$ as a sacrificial template and nitrogen-rich polymer to obtain nitrogen-doped graphene and then anchored the rich Co atomic sites on the nitrogen-doped graphene to prepare the CoN$_4$–G support. Finally, by adsorbing [PtCl$_6$]$^{2-}$ on the CoN$_4$–G support and annealing at 400 °C in a 5% H$_2$/Ar atmosphere, the Pt@CoN$_4$–G catalyst was obtained (Fig. 5d).[113] The prepared Pt@CoN$_4$–G still maintains the wrinkled nanosheet morphology and abundant nanopores, which can provide a large surface area, abundant defective active sites, and mass transfer channels, thereby promoting the catalytic reaction. Fig. 5e verifies that the Pt clusters are surrounded by dense bright spots with two different contrasts; the brighter spots and darker spots can be

identified as isolated Pt atoms and Co atoms, respectively, further proving that the Pt species are anchored on graphene. Nevertheless, characterization results show the coexistence of Pt single atoms and Pt clusters in the system, indicating that the adsorption amount of Pt lacks clear quantitative regulation, which reflects the randomness of the current synthesis scheme at the atomic scale. Benefiting from the SMSI between the Pt species and the CoN_4–G support and the synergistic effect of multiple active sites, it manifests fine HER activity (η_{10} = 39 mV) and stability under alkaline electrolytes (Fig. 5f). Similarly, Guo's group anchored triphenylphosphine (PPh₃)-coordinated Pt_6 clusters to isolated Cr–N_4 sites (Cr–N–C) on mesoporous carbon substrates through a simple wet impregnation process, followed by heat treatment to remove surface ligands to synthesize Pt–AC/Cr–N–C catalysts (Fig. 5g).[114] Transmission electron microscopy (TEM) images of the prepared Pt–AC/Cr–N–C reveal that it is a 2D ultrathin sheet structure without visible metal NPs. Instead, most of the sub-nanometer (<1 nm) sized Pt atomic clusters are dispersed on the carbon substrate (Fig. 5h and inset). Combined with DFT, it was demonstrated that the unique Pt–Cr quasi-covalent interaction formed at the interface between the Cr–N_4 site and the Pt ACs effectively suppressed the migration and thermal vibration of Pt atoms, stabilized the Pt atomic clusters, and exhibited a very low overpotential of only 19 mV to reach 10 mA cm^{-2} (Fig. 5i). In addition, an AEMWE using this catalyst (with only 50 μg_{Pt} cm^{-2}) can operate stably at an industrial-level

current density of 500 mA cm^{-2} at 1.8 V for >100 h with a small degradation rate of 90 μV h^{-1}. The previous studies have offered a constructive approach for the precise design of single Pt-based robust electrocatalysts with high HER activity and durability. However, this approach, despite its simplicity and scalability, has a lengthy reaction time, which may result in the agglomeration of Pt NPs, damage to the carbon matrix's pore structure, and a decrease in surface area.

Beyond the thermally induced reduction of precious metal Pt, the intrinsic defects of carbon carriers can also be harnessed for the reduction process. More precisely, the inherent defects within the carbon carrier, including vacancies and lattice distortion, serve as active sites. These sites enable the reduction of precious metal Pt from its compounds, such as oxides and salts, to the metallic state via chemical or physical interactions.[115] This approach leverages the electronic properties of defects or the local chemical environment, eliminating the need for strong reducing agents, characterized by its eco-friendliness, high efficiency, and exceptional controllability.[116] Nonetheless, it is constrained by the difficulty of precisely controlling defect density and distribution, and the reduction efficiency is limited by the electron-supplying capacity of the carrier's intrinsic defects.[117]

For instance, Luo et al. synthesized porous carbon supports (TC) featuring varying levels of inherent defects employing a straightforward template-assisted methodology. Subsequently, they deposited Pt onto these carbon supports to fabricate a
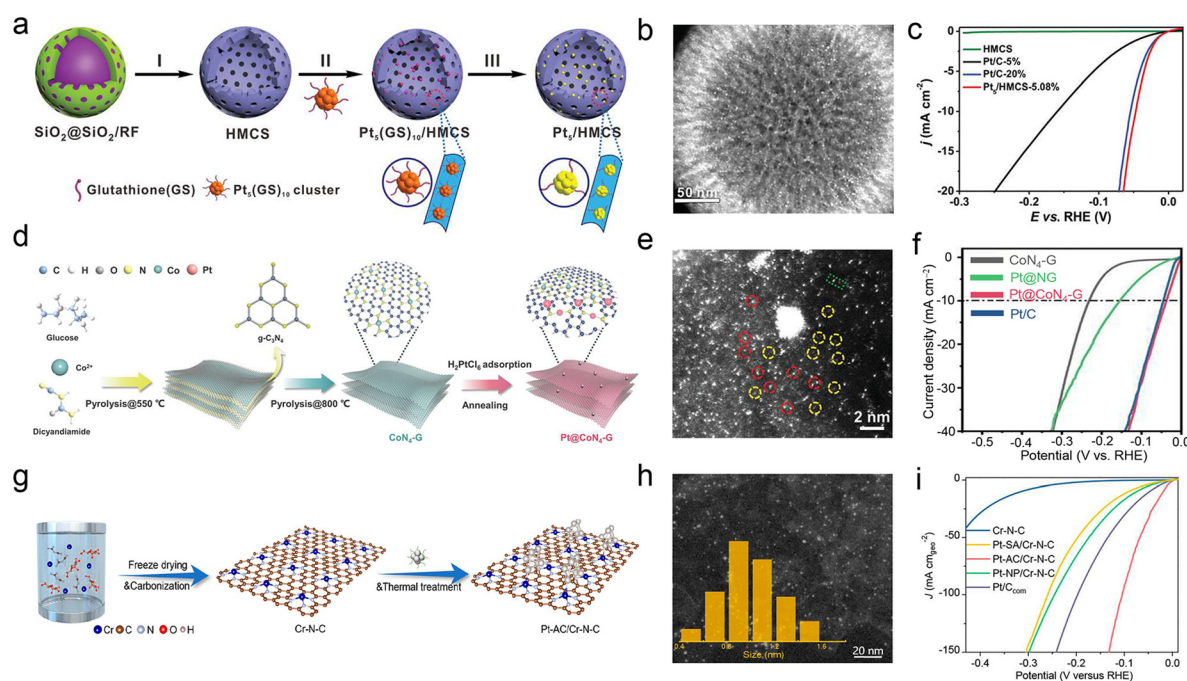
Fig. 5 (a) Schematic illustration of the synthetic procedure of Pt_5/HMCS. Step I: carbonization and etching of SiO_2 to form HMCS. Step II: load the $Pt_5(GS)_{10}$ clusters into HMCS to form $Pt_5(GS)_{10}$/HMCS. Step III: conversion of $Pt_5(GS)_{10}$/HMCS to Pt_5/HMCS electrocatalyst through thermal treatment. (b) HAADF-STEM image. (c) LSV curves of Pt_5/HMCS-5.08% and commercial Pt/C (5 and 20 wt%) catalysts based on the geometric area of the working electrode in 1.0 M KOH. Reproduced with permission.[112] Copyright 2019, Wiley-VCH GmbH. (d) Synthetic illustration of the synthetic process for Pt@CoN_4–G. (e) Aberration-corrected HAADF-STEM image. Single Co atoms are marked by yellow circles, and single Pt atoms are marked by red circles. (f) LSV curves of different electrocatalysts in 1.0 M KOH. Reproduced with permission.[113] Copyright 2023, Wiley-VCH GmbH. (g) Schematic illustration of the preparation of Pt–AC/Cr–N–C. (h) HAADF-STEM image. Inset, the size distribution of Pt ACs. (i) LSV curves tested in 1 M KOH solution. Reproduced with permission.[114] Copyright 2023, American Chemical Society.

range of Pt/TC catalytic materials.[118] The findings demonstrate that the plentiful inherent defects (such as vacancies and topological defects) in the carbon supports are beneficial for the dispersion and anchoring of Pt species. Meanwhile, it also facilitates the electron transfer between Pt atoms and the carbon supports and modulates the electronic state of Pt species. These properties enhance the HER performance of the Pt/TC catalysts, which display a lower overpotential of 58 mV at a current density of 10 mA cm^{-2}. DFT calculations verify that intrinsic defects, including vacancies and topological defects, play a crucial role in stabilizing Pt atoms. Among them, the Pt–C3 coordination is regarded as the most advantageous structure for enhancing the hydrogen evolution performance of Pt. This research offers fresh perspectives on the significant contribution of the inherent defects within the porous carbon supports to the HER performance of the Pt/C catalysts. Such insights are of profound importance for the future design and fabrication of advanced carbon-supported catalysts as well as other carbon-based electrode materials. Besides, Zhang *et al.* used C$_{60}$ as an electron-accepting carrier to anchor Pt atoms and synthesized a highly loaded and highly dispersed Pt catalyst (Pt/C$_{60}$) at room temperature.[119] The resultant catalyst has a Pt loading as high as 21 wt%, predominantly comprising Pt SAs with a minor fraction of Pt clusters. This composition endows it with excellent HER catalytic activity, showing an overpotential of merely 25 mV at 10 mA cm^{-2} in 1 M KOH solution.

In the construction system of carbon-supported Pt-based catalysts, the carbon reduction method primarily achieves the controllable loading and stable anchoring of active Pt species through two pathways: pyrolysis-assisted reduction and defect-induced reduction. The pyrolysis-assisted reduction strategy leverages high-temperature pyrolysis processes to drive the highly uniform dispersion of Pt species in the form of single atoms or sub-nanometer clusters, effectively enhancing the atomic utilization efficiency of precious metal Pt. Nevertheless, this method relies on high-temperature energy consumption, which not only increases the energy cost during the preparation process but also makes the ligand removal step prone to causing the collapse or reconstruction of the pore structure of the carbon support. This, in turn, disrupts the continuity and effectiveness of the mass transfer channels, potentially negatively impacting the catalytic performance. In contrast, the defect-induced reduction pathway delves into the intrinsic electronic properties of the inherent structural defects (including lattice vacancies, topological distortions, *etc.*) of the carbon support. It realizes an *in situ* reduction process through charge transfer between the defect sites and Pt precursors, avoiding the use of external chemical reducing agents and conforming to the concept of green synthesis. In this process, the structural defects on the surface of the carbon support act as active anchoring sites, which effectively suppress the migration and agglomeration behaviors of Pt species through interfacial electron interactions, thereby achieving uniform dispersion of ultra-small Pt NPs on the support surface. Nevertheless, this strategy faces two major technical challenges: first, there is a lack of precise control methods for the density and spatial distribution of carbon support defects, making it difficult to achieve a quantitative match between defect sites and Pt loading; second, the intrinsic electron-donating ability of carbon materials becomes a key factor limiting the reduction efficiency, resulting in the inability to optimize the reduction degree and loading of Pt species. Therefore, innovative material design and synthesis process improvements are urgently needed to overcome the existing technical bottlenecks.

4.2. Chemical reduction method

Chemical reduction is a method of reducing metal ions (or other high-valent substances) to metal elements or low-valent compounds through chemical reactions. The core of the method is to use a reducing agent to provide electrons so that the target substance can obtain electrons and reduce its valence.[120] The reaction conditions are mild, and the size and morphology of the product (such as NPs and clusters) can be controlled by adjusting the type and concentration of the reducing agent. Nevertheless, some reducing agents have the disadvantages of being expensive or toxic and possibly introducing impurities.[121]

In the field of preparing carbon-supported Pt-based catalysts, the chemical reduction method is primarily realized through two pathways: the first involves introducing non-noble metals and leveraging the redox potential difference to promote the formation of Pt particles, ultimately constructing PtM alloy catalysts; the second employs strong reducing agents such as NaBH$_4$ to achieve the reduction and preparation of Pt particles.

For example, Xiao *et al.* used the difference in redox potential between metals to direct the replacement of ions to prepare ultrafine Pt confined in N-doped porous carbon fibers (Pt@NDPCF).[122] Specifically, imidazole ligands can coordinate with Zn ions to form ordered porous MOF materials, and then the 0D MOF particles are aggregated into 1D fibers by electrospinning technology, followed by carbonization to obtain highly confined Zn (0) in N-doped hierarchical porous carbon fibers (Zn@NDPCF). Due to the large difference between the redox potentials of Pt(II)/Pt (+1.2 V) and Zn(II)/Zn (−0.76 V), Zn (0) in Zn@NDPCF can be easily replaced by Pt at room temperature to form Pt@NDPCF. This synthetic strategy can form highly dispersed ultrafine Pt–NPs with strong directional interactions between Pt and pyridinic N, which significantly enhances the heavy d–π effect and greatly improves the HER activity (η_{10} = 36 mV) and durability. Although this system inhibits agglomeration through nitrogen-doped carbon carriers, it has not completely solved the problem of intrinsic thermodynamic instability. Similarly, Zhang *et al.* loaded ultrafine Pt–Co alloy NPs (designated Pt–Co@NCNT) on the inner and outer shells of porous nitrogen-doped carbon nanotubes *via* a pyrolysis-replacement-reorganization strategy (Fig. 6a).[123] That is, the Co confined in the N-doped CNTs (Co@NCNTs) undergoes a galvanic replacement reaction with a K$_2$PtCl$_4$ solution, and then the PtCl$_4^{2-}$ is replaced by Co NPs and forms Pt–Co NPs with additional Co NPs, confined in the porous N-doped carbon nanotubes (denoted as pre-Pt–Co@NCNT, Fig. 6b). The Pt–Co@NCNT electrocatalyst obtained by further

thermal annealing reorganization can drive a current density of 10 mA cm^{-2} at an overpotential of only 20 mV in alkaline media (Fig. 6c), exhibiting over 100 h HER stability. Xu et al. proposed a simple pyrolysis-confinement strategy to synthesize Co$_n$–Pt$_1$@NPC catalysts, where Co nano-metal-particles (Co$_n$) and Pt SA (Pt$_1$) were co-confined in N-doped lantern-shaped hollow polyhedral carbon materials (Fig. 6d).[124] First, ZIF-8@ZIF-67 (Co/Zn zeolitic imidazolate framework) with a core–shell structure was pyrolyzed as a precursor to generate hollow polyhedral porous carbon materials (Co$_n$@NPC) loaded with Co NPs as a carrier. Then, Co$_n$@NPC was immersed in H$_2$PtCl$_6$ solution, and driven by the difference in reduction potentials of Co and Pt ions, the Pt ions were reduced. Fig. 6e confirms that Co NPs coexist with Pt atoms, and Pt mainly falls on the carbon surface without destroying the Co lattice. This strategy can regulate the metal content and size of the NPs and has excellent HER activity in 1 M KOH solution (η_{10} = 20 mV, Fig. 6f). Whether it is Zn substitution in Zn@NDPCF or Co reduction in Co$_n$@NPC, an excess of sacrificial metal is consumed, resulting in a loss of loading efficiency of the precious metal Pt.

Besides, Chen et al. first prepared buckminsterfullerene (C$_{60}$) bulk crystals by a modified liquid–liquid interface precipitation method, and then added NaBH$_4$ to reduce H$_2$PtCl$_6$ (Fig. 6g).[125] The formed Pt clusters induced the one-step exfoliation of C$_{60}$ crystals to prepare Pt nanocluster catalysts on C$_{60}$ nanosheets (Pt/C$_{60}$). During the exfoliation process, the reduction of H$_2$PtCl$_6$ precursor with NaBH$_4$ can successfully

surpass the interlayer interactions existing in C$_{60}$ bulk crystals along the [110] axis, facilitating the achievement of the targeted PtC$_{60}$ nanosheets (Fig. 6h). As a result, the lattice distance of the fullerene nanosheets is unusually large ($\sim$0.8 nm), while the size of the Pt clusters is extremely small ($\sim$2 nm), resulting in strong confinement of the Pt clusters and a remarkable charge redistribution at the tight Pt/fullerene interface, attaining the current densities of 10 mA cm^{-2}, 50 mA cm^{-2}, and 150 mA cm^{-2} at overpotentials of 24.3 mV, 53.2 mV, and 110.0 mV, respectively (Fig. 6i). These studies provide new inspiration in relation to the design of Pt-based nanomaterials boasting high performance.

Relying on the electron transfer properties of chemical reducing agents or the mechanism of intermetallic displacement reactions, the chemical reduction method exhibits remarkable advantages such as strong operational adaptability and a well-established process system, enabling the controllable preparation of nanoscale Pt particles. However, this method still faces two major technical bottlenecks in practical applications. On the one hand, the issues of reducing agent residue and nanoparticle aggregation urgently need to be addressed. The former may introduce impurities that affect catalytic performance, while the latter leads to insufficient exposure of active sites. On the other hand, whether by introducing other metal atoms to create displacement reaction conditions or directly adding chemical reducing agents, raw material loss is inevitable. Compared with pyrolysis processes, Pt NPs prepared by the chemical reduction method generally have larger average particle sizes, which
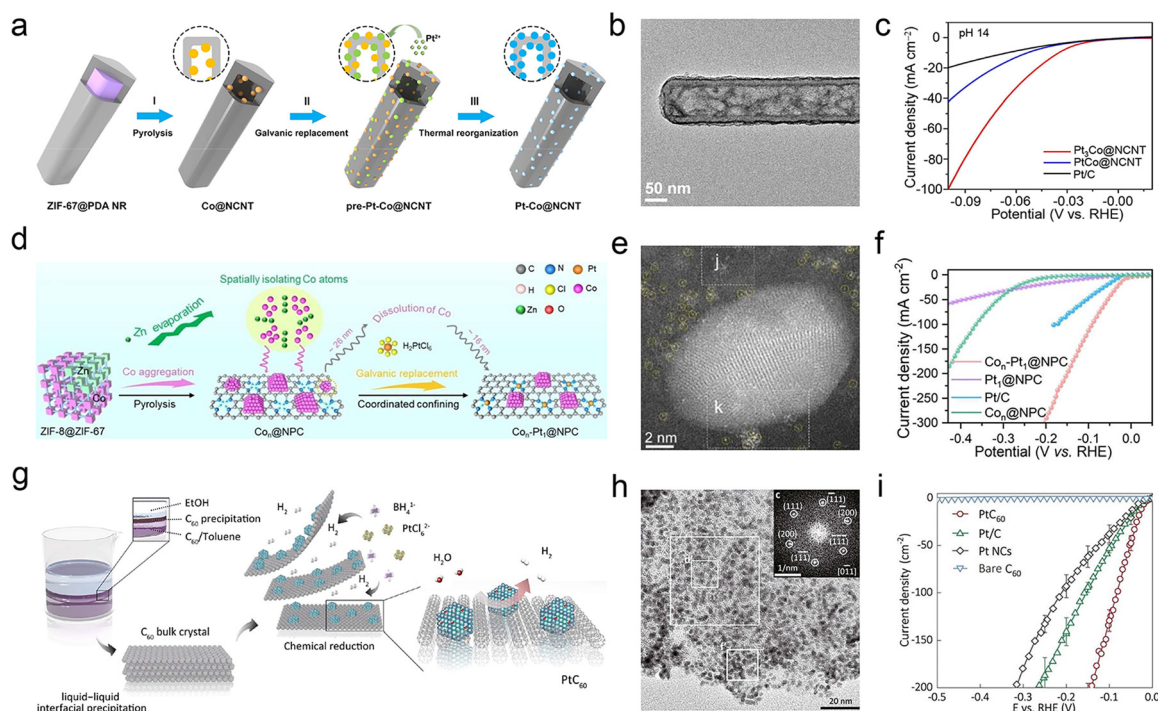
Fig. 6 (a) Illustration of the synthesis of Pt–Co@NCNT. (b) TEM image of a pre-Pt$_3$Co@NCNT. (c) LSV curves tested in 1 M KOH solution. Reproduced with permission.[123] Copyright 2021, Wiley-VCH GmbH. (d) Synthesis of Co$_n$–Pt$_1$@NPC via a pyrolysis-confinement strategy. (e) HAADF-STEM image of Co$_n$–Pt$_1$@NPC. (f) Polarization curves of Pt–Co@NCNT, Pt$_1$@NPC, Co$_n$@NPC and 20%Pt/C. Reproduced with permission.[124] Copyright 2025, Wiley-VCH GmbH. (g) Schematic of the synthetic route of PtC$_{60}$. (h) TEM image of PtC$_{60}$. (i) LSV of Pt catalysts with the loading of 0.4 mg cm^{-2} and bare C$_{60}$. Reproduced with permission.[125] Copyright 2023, Nature.

directly reduces the surface utilization rate of Pt atoms and thus limits their efficient application in the field of catalysis. To sum up, reduction reactions using reducing agents provide important ideas and methodological guidance for the efficient regulation of the morphology and structure of catalysts. However, it should not be overlooked that there is still room for optimization of this technology. Future research can focus on three core directions: the development of green reducing agents, the efficiency of catalyst preparation processes, and the precise regulation of active sites.

4.3. Electroreduction and photoreduction methods

Electroreduction and photoreduction are techniques that harness electrical energy or light energy to drive electron transfer, thereby reducing oxidized metals to their metallic states. Electroreduction has numerous advantages: (1) the composition, structure, and even crystal face exposure of the material can be precisely controlled by adjusting the electrolyte composition/pH, deposition potential/current, and temperature; (2) electrochemical reduction allows the active material to grow directly on a conductive substrate, which is beneficial for electron transfer and active site utilization; (3) electrochemical reduction is low-cost, high-purity and environmentally friendly.[126,127] In electrochemical reduction techniques, electrodeposition is the most prevalent and paradigmatic approach, which is a technology that applies an electric current to an electrolyte solution and deposits metals or other materials onto conductive substrates through electrochemical reactions.[128,129] Electrochemical deposition, by virtue of external electric fields, enables precise control over Pt loading and nanostructures, making it particularly suitable for the preparation of single-atom catalysts. Moreover, the resultant Pt NPs exhibit uniform dispersion, robust adhesion to the carbon matrix, and outstanding stability, rendering them highly suitable for alkaline HER.

Wang's group used cathodic electrochemical deposition to synthesize PtRu bimetallic clusters with adjacent SnO_{2-x} on the CNT ($PtRu/CNT@SnO_{2-x}$) catalyst (Fig. 7a).[130] As shown in Fig. 7b, the PtRu alloy was deposited on the carbon nanotubes. They investigated the effect of SnO_2 loading on the conductivity and metal site deposition of $CNT@SnO_{2-x}$ and concluded that CNTs and SnO_{2-x} multi-sites synergistically promoted alkaline HER kinetics, exhibiting an overpotential of only 75 mV at 100 mA cm^{-2} in 1 M KOH (Fig. 7c). However, this method uses non-conductive carriers and requires pre-modification of conductive layers (such as SnO_{2-x}), which increases the process steps. Moreover, when the PtRu alloy is electrolyzed for a long time at 1 M KOH, the Ru component may dissolve out, resulting in overpotential drift. Li et al. synthesized Pt-doped Co on carbon cloth (CC) by co-electrodeposition of CoPt alloy, and then successfully obtained $Pt–Co_2P$ particles ($Pt–Co_2P/CC$) grown on CC by phosphating (Fig. 7d).[131] Scanning electron microscopy (SEM) confirmed that $Pt–Co_2P$ particles with a size distribution between 125 nm and 150 nm were uniformly grown on CC (Fig. 7e). By internally modifying Co_2P via electrodeposition of Pt, the local chemical state and electronic structure of the catalyst can be tuned to enhance electron mobility and reduce the energy barriers for hydrogen

adsorption and H–H bond formation, significantly improving the HER activity under alkaline conditions, with a much lower overpotential of 2 mV to achieve 10 mA cm^{-2} (Fig. 7f), which is superior to the performance of a great majority of current alkaline HER catalysts. But it cannot be ignored that during the co-electrodeposition of CoPt alloys, the excess Co^{2+} residue may form hydroxide precipitates, blocking the active sites.

Similarly, photoreduction, as a green synthesis strategy, involves a metal precursor reduction process driven by photo-induced electron transfer, which mainly includes three kinetic regulation stages: controllable nucleation, directional growth, and final conversion into stable metal NPs.[111] This method precisely anchors highly dispersed metal NPs on the surface of carbon carriers through photochemical reduction. Moreover, by reducing the reaction nucleation rate, uniformly dispersed metal clusters or single atoms can be prepared. At the same time, the use of low-temperature light sources such as ultraviolet rays can effectively prevent the aggregation of metal atoms.[133] For example, Yao's group prepared Pt@DG catalysts with rich Pt–C3 coordination structures by photoreducing H_2PtCl_6 on defective graphene (DG).[132] As demonstrated in Fig. 7g, the mixture of melamine and graphene was first pyrolyzed at 700 °C for 2 h to obtain N-doped graphene (NG), and DG was formed by annealing NG at 1150 °C to completely remove N species. Finally, Pt^{4+} was uniformly dispersed on DG and then photoreduced to obtain Pt@DG. Many bright dots are observed to distribute evenly on the graphene surface from high-magnification HAADF-STEM (Fig. 7h), indicating the successful formation of atomic Pt. Experimental and theoretical results confirm that the optimal Pt–C3 coordination structure has a stronger electron capture ability and lower ΔG, which promotes the reduction of adsorbed H$^+$ and the desorption rate of H$_2$, thus exhibiting excellent HER activity (Fig. 7i). Furthermore, Ji et al. used photoreduction to synthesize both Pt single atom/cluster anchored functional multi-walled CNTs (Pt/f-MWCNTs), which exhibit the overpotential of 43.9 mV at a current density of 10 mA cm^{-2}.[134] Photoreduction technology is limited by the penetration depth of ultraviolet light less than 100 μm and is only suitable for thin-layer materials such as defective graphene. It is prone to cause uneven reduction on thick substrates such as bulk carbon carriers.

Electroreduction and photoreduction technologies have provided unique technical pathways and innovative strategies for the controllable synthesis and performance optimization of catalysts. By driving electron transfer through electrical or light energy, precise regulation of material structures and active sites can be achieved. Although the above technologies have demonstrated remarkable advantages in basic research, their industrial applications still face multiple bottlenecks. The electroreduction process is constrained by its high energy consumption, and electrode materials are prone to structural collapse and active component loss during long-term cycling, leading to catalytic performance degradation. Additionally, in the preparation of large-area catalysts, the non-uniform distribution of electric fields inevitably causes spatial differences in active site distribution, affecting the overall performance
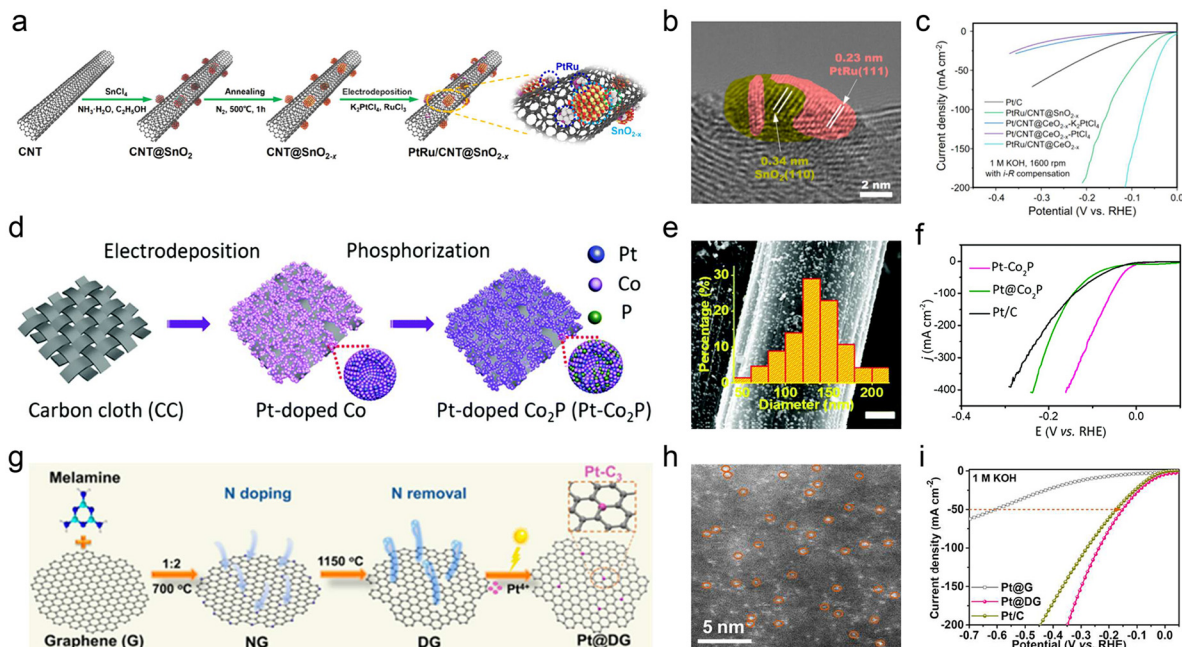
Fig. 7 (a) Schematic diagram of the preparation process of the M/CNT@SnO$_{2-x}$ catalyst. (b) HRTEM image of PtRu/CNT@SnO$_{2-x}$. The yellow marked area belongs to the SnO$_{2-x}$ nanoparticle, and the pink area represents the electrodeposited Pt and Ru. (c) HER polarization curves for commercial Pt/C, Pt/CNT@SnO$_{2-x}$–K$_2$PtCl$_4$, Pt/CNT@SnO$_{2-x}$–PtCl$_4$, and PtRu/CNT@SnO$_{2-x}$ in 1 M KOH solution at a scan rate of 10 mV s^{-1}. Reproduced with permission.[130] Copyright 2024, American Chemical Society. (d) Schematic illustration of the fabrication process of Pt–Co$_2$P. (e) SEM image of Pt–Co$_2$P particles grown on CC. The inset is the particle size distribution. Scale bar: 2 μm. (f) LSV curves of the catalysts tested at 5 mV s^{-1}. Reproduced with permission.[131] Copyright 2020, The Royal Society of Chemistry. (g) Schematic illustration of the preparation of Pt@DG. (h) HAADF-STEM image of Pt@DG. (i) Polarization curves of Pt@G, Pt@DG, and Pt/C with a scan rate of 10 mV s^{-1}. Reproduced with permission.[132] Copyright 2022, American Chemical Society.

consistency of the catalytic system. The practical application of photoreduction technology is limited by the theoretical upper limit of light absorption efficiency: existing photocatalysts have a narrow response range to the solar spectrum, and the rapid recombination of photogenerated carriers seriously reduces energy conversion efficiency. Meanwhile, the complex photophysical and photochemical reaction processes in photoreduction systems, as well as the interaction mechanisms between photocatalysts and reaction media, further increase the difficulty of regulating the reaction process. For future development, there is an urgent need to develop novel catalytic systems driven by the synergistic effect of electrical and light energy. By constructing a photoelectro-coupled reaction interface, the complementary advantages of the two energy forms can be realized. This strategy is expected not only to break through the performance bottlenecks of single-energy input modes but also to provide new ideas for catalyst structure design and performance regulation, thereby promoting the large-scale application of electroreduction and photoreduction technologies in fields such as energy catalysis and environmental remediation.

To sum up, the interaction between carbon supports and Pt significantly enhances the activity and stability of carbon-supported Pt-based catalysts for alkaline HER, as demonstrated in three aspects: (1) the specific surface area, porous architecture, and defect sites of carbon supports provide dispersion sites for Pt, effectively inhibiting agglomeration. (2) Surface functionalization and heteroatom doping (*e.g.*, N/P/S) modulate the electronic structure of supports, strengthening interfacial

coupling with Pt and optimizing H* adsorption kinetics as well as H$_2$O dissociation dynamics. (3) The mechanical and chemical stability of 3D carbon materials suppresses Pt dissolution and agglomeration in alkaline media, extending catalyst lifespan. Such interactions synergistically boost catalytic activity through structural matching, electronic modulation, and interfacial reinforcement. Meanwhile, heteroatom doping and 3D structural design enhance stability *via* chemical bonding and skeletal support, paving the way for the development of low-Pt-loading catalysts.

5. Conclusion and perspective

This review briefly summarizes the factors that affect the slow kinetics of alkaline water electrolysis and focuses on elucidating the latest progress in the regulation of carbon substrates and synthesis methods. Despite notable advancements in enhancing the efficacy of Pt-based catalysts for the HER under alkaline conditions, persisting challenges remain, particularly concerning the high cost attributed to low Pt atom utilization and inadequate long-term durability. Consequently, further investigations are imperative to address the following issues for the widespread deployment of carbon-supported Pt-based electrocatalysts.

5.1. Selecting the optimal carbon support

Currently, traditional carbon supports struggle to meet the demands of high-performance catalysis and energy storage

due to weak interactions with active components and monotonous structures. Future research should focus on novel carbon materials like fullerenes, graphynes, and porous carbon nanosheets. Exploring their electronic and surface properties, and using advanced techniques to precisely control the microstructure and pores of carbon supports, will enhance the synergy with active substances. This will help screen high-performance, adaptable carbon supports, driving technological progress in related fields.

5.2. Improving long-term stability

Under harsh conditions of extreme pH and high current densities, carbon matrices risk structural collapse, with noble-metal active sites' inactivation during electrolysis, shortening material lifespans. To address this, innovation in material design is crucial. Firstly, refined structural designs are needed for research and development. For instance, the implementation of *in situ* encapsulation techniques to embed Pt NPs within carbon-based supports enables the fabrication of stable core–shell architectures to protect active sites from alkaline erosion and facilitates electron transfer. Secondly, metal–oxide modification of carbon matrices should be further explored to create stable Pt–M–C bonds. This can optimize active-site charge distribution by adjusting interfacial electronic structures to reduce noble-metal oxidation and enhance catalyst durability.

5.3. Understanding the HER mechanism and exploring dynamic structure–activity relationships

Although extensive progress has been made in the research of the structure–activity relationship, there are still significant deficiencies in exploring the dynamic evolution behavior of catalysts during the reaction in alkaline HER. In actual reactions, the structure and morphology of catalysts are in a continuous dynamic change process. It is urgent to utilize advanced *in situ* characterization techniques, such as *in situ* X-ray absorption spectroscopy (*in situ* XAS) and *in situ* X-ray diffraction (*in situ* XRD), to analyze the dynamic structure–activity relationship between the catalysts and their performance during the reaction. Future research should combine the pre-design of the catalyst structure with the regulation of its dynamic evolution to achieve efficient dynamic regulation of the catalyst structure. Eventually, the structure–activity relationship between the catalyst structure design, the dynamic evolution of the catalyst, and the catalytic performance can be clarified.

5.4. Developing practical electrocatalytic systems

At electrocatalysis' critical industrialization stage, electrolyte innovation and resource recycling are key to overcome practical and economic barriers. New electrolytes will focus on improving system compatibility and stability, using composite electrolytes to optimize interfaces and reduce side reactions, while exploring solid electrolytes to solve leakage issues. For resource recycling, a highly selective catalytic system is needed to recycle industrial waste and salt/corrosion-resistant materials should be developed to break through the technical bottlenecks of seawater electrolysis. Building a green, low-cost recycling system will accelerate electrocatalysis' large-scale adoption, advancing the "dual carbon" goals.

5.5. Establishing measurement and evaluation standards

For membrane electrode assemblies (MEA), the lack of unified testing standards has become the core bottleneck for industrial promotion. The inconsistent specifications of electrode areas, the wide range of testing temperatures, the absence of standardized processes for synthesis techniques, as well as the lack of unified specifications for the selection of carbon papers and adhesives, have made it difficult to compare the test data and resulted in poor reliability of the test results. It is urgently necessary for industry experts, research institutions, and enterprises to collaborate in formulating comprehensive standards. Through standardization efforts, the comparability and reliability of the data can be enhanced, and the industrialization process of MEA can be accelerated.

5.6. Optimizing the design of the electrolytic cell

In practical applications of alkaline HER, the alkaline electrolyte readily reacts with CO_2 in the air to form CO_3^{2-}, which deposits on the catalyst surface, blocking the active sites and reducing the reaction efficiency. Meanwhile, in the MEA, the carbon support and the ion-exchange membrane experience interfacial separation under alkaline conditions due to chemical degradation, mechanical stress, *etc.*, increasing the mass transfer resistance and posing leakage risks. Additionally, under dynamic operating conditions with frequent fluctuations in current density (such as when matching solar or wind power generation), the activity of the catalyst and the lifespan of the electrolyzer are vulnerable, and the system requires the development of intelligent control strategies to adapt to power fluctuations, further increasing the difficulty of system design.

Conflicts of interest

The authors declare no conflict of interest.

Data availability

The data that support the findings of this study are available from the corresponding author upon reasonable request.

Acknowledgements

References

1 J. Zhang, C. Ma, S. Jia, Y. Gu, D. Sun, Y. Tang and H. Sun, *Adv. Energy Mater.*, 2023, **13**, 2302436.
2 Z. Chen, N. Han, W. Wei, D. Chu and B. Ni, *EcoEnergy*, 2024, **2**, 114–140.

© 2025 The Author(s). Published by the Royal Society of Chemistry

3 X. Hu, B. Yang, S. Ke, Y. Liu, M. Fang, Z. Huang and X. Min, *Energy Fuels*, 2023, **37**, 11532–11566.

4 L. Quan, H. Jiang, G. Mei, Y. Sun and B. You, *Chem. Rev.*, 2024, **124**, 3694–3812.

5 C. Acar and I. Dincer, *Int. J. Hydrogen Energy*, 2020, **45**, 3396–3406.

6 E. Shagdar, B. G. Lougou, Y. Shuai, E. Ganbold, O. P. Chinonso and H. Tan, *RSC Adv.*, 2020, **10**, 12582–12597.

7 S. Saeidi, A. Sápi, A. H. Khoja, S. Najari, M. Ayesha, Z. Kónya, B. B. Asare-Bediako, A. Tatarczuk, V. Hessel, F. J. Keil and A. E. Rodrigues, *Renewable Sustainable Energy Rev.*, 2023, **183**, 113392.

8 W. Ma, X. Zhang, W. Li, M. Jiao, L. Zhang, R. Ma and Z. Zhou, *Nanoscale*, 2023, **15**, 11759–11776.

9 J. Zheng, W. Sheng, Z. Z. Xu and Y. Yan, *Sci. Adv.*, 2016, **2**, e1501602.

10 C. Li and J. Baek, *ACS Omega*, 2019, **5**, 31–40.

11 G. Gao, G. Zhu, X. Chen, Z. Sun and A. Cabot, *ACS Nano*, 2023, **17**, 20804–20824.

12 Y. Liu, Q. Wang, J. Zhang, J. Ding, Y. Cheng, T. Wang, J. Li, F. Hu, H. B. Yang and B. Liu, *Adv. Energy Mater.*, 2022, **12**, 2200928.

13 M. Chatenet, B. G. Pollet, D. R. Dekel, F. Dionigi, J. Deseure, P. Millet, R. D. Braatz, M. Z. Bazant, M. Eikerling, I. Staffell, P. Balcombe, Y. Shao-Horn and H. Schäfer, *Chem. Soc. Rev.*, 2022, **51**, 4583–4762.

14 I. T. McCrum and M. T. M. Koper, *Nat. Energy*, 2020, **5**, 891–899.

15 F. Yang, Y. Wang, Y. Cui, X. Yang, Y. Zhu, C. M. Weiss, M. Li, G. Chen, Y. Yan, M. D. Gu and M. Shao, *J. Am. Chem. Soc.*, 2023, **145**, 27500–27511.

16 M. Jiang, J. Xu, Q. Zhou, Y. Chen, P. Munroe, L. Li, Z. Xie, Y. Wu and S. Peng, *Angew. Chem., Int. Ed.*, 2025, e202510259, DOI: 10.1002/anie.202510259,.

17 C. Shu, J. Cao, Z. Gan, P. Qiu, Z. Chen, L. Guanwu, Z. Chen, C. Deng and W. Tang, *Mater. Futures*, 2024, **3**, 035101.

18 C. Wan, Z. Zhang, S. Wang, Q. Sun, E. Liu, H. Pu, A. Zhang, Z. Chen, A. H. Shah, X. Fu, A. N. Alexandrova, Q. Jia, Y. Huang and X. Duan, *J. Am. Chem. Soc.*, 2025, **147**, 12162–12169.

19 C. Hu, L. Zhang and J. Gong, *Energy Environ. Sci.*, 2019, **12**, 2620–2645.

20 J. Guo, J. Huo, Y. Liu, W. Wu, Y. Wang, M. Wu, H. Liu and G. Wang, *Small Methods*, 2019, **3**, 1900159.

21 G. Patil, S. Daniel and K. S. Lokesh, *Int. J. Hydrogen Energy*, 2024, **86**, 104–113.

22 H. Huang, M. Yan, C. Yang, H. He, Q. Jiang, L. Yang, Z. Lu, Z. Sun, X. Xu, Y. Bando and Y. Yamauchi, *Adv. Mater.*, 2019, **31**, 1903415.

23 C. T. Campbell, *Nat. Chem.*, 2012, **4**, 597–598.

24 A. K. Mrinalini Kalyani, R. Rajeev, L. Benny, A. R. Cherian and A. Varghese, *Mater. Today Chem.*, 2023, **30**, 101523.

25 S. M. Thalluri, J. RodriguezPereira, R. Zazpe, B. Bawab, E. Kolíbalová, L. Jelinek and J. M. Macak, *Small*, 2023, **19**, 2300974.

26 J. Yang, W. Shi, Q. Xu, X. Yin and P. Zelenay, *ACS Catal.*, 2023, **13**, 14953–14964.

27 X. Ma, T. Wang, B. Gong and H. Cao, *J. Power Sources*, 2024, **623**, 235479.

28 K. Hayashida, J. Nakamura and K. Takeyasu, *Angew. Chem., Int. Ed.*, 2025, e202502702, DOI: 10.1002/anie.202502702.

29 X. Sui, L. Zhang, J. Li, K. Doyle-Davis, R. Li, Z. Wang and X. Sun, *Adv. Energy Mater.*, 2021, **12**, 2102556.

30 J. Wang, H. Kong, J. Zhang, Y. Hao, Z. Shao and F. Ciucci, *Prog. Mater. Sci.*, 2021, **116**, 100717.

31 J. Wei, M. Zhou, A. Long, Y. Xue, H. Liao, C. Wei and Z. J. Xu, *Nano-Micro Lett.*, 2018, **10**, 75.

32 N. Mahmood, Y. Yao, J. Zhang, L. Pan, X. Zhang and J. J. Zou, *Adv. Sci.*, 2017, **5**, 1700464.

33 X. Zou and Y. Zhang, *Chem. Soc. Rev.*, 2015, **44**, 5148–5180.

34 H. Sun, M. Chen, B. Xiao, T. Zhou, M. Humayun, L. Li, Q. Lu, J. He, J. Zhang, M. Bououdina, C. Wang and Q. Liu, *Small*, 2023, **19**, 2303974.

35 H. Tan, B. Tang, Y. Lu, Q. Ji, L. Lv, H. Duan, N. Li, Y. Wang, S. Feng, Z. Li, C. Wang, F. Hu, Z. Sun and W. Yan, *Nat. Commun.*, 2022, **13**, 2024.

36 J. Dai, Y. Zhu, Y. Chen, X. Wen, M. Long, X. Wu, Z. Hu, D. Guan, X. Wang, C. Zhou, Q. Lin, Y. Sun, S.-C. Weng, H. Wang, W. Zhou and Z. Shao, *Nat. Commun.*, 2022, **13**, 1189.

37 X. Chen, I. T. McCrum, K. A. Schwarz, M. J. Janik and M. T. M. Koper, *Angew. Chem., Int. Ed.*, 2017, **56**, 15025–15029.

38 R. Subbaraman, D. Tripkovic, K. Chang, D. Strmcnik, A. P. Paulikas, P. Hirunsit, M. Chan, J. Greeley, V. Stamenkovic and N. M. Markovic, *Nat. Mater.*, 2012, **11**, 550–557.

39 N. Danilovic, R. Subbaraman, D. Strmcnik, K. Chang, A. P. Paulikas, V. R. Stamenkovic and N. M. Markovic, *Angew. Chem., Int. Ed.*, 2012, **51**, 12495–12498.

40 R. Subbaraman, D. Tripkovic, D. Strmcnik, K.-C. Chang, M. Uchimur, A. P. Paulikas, V. Stamenkovic and N. M. Markovic, *Science*, 2011, **334**, 2.

41 W. Sheng, Z. Zhuang, M. Gao, J. Zheng, J. G. Chen and Y. Yan, *Nat. Commun.*, 2015, **6**, 5848.

42 Y. Zheng, Y. Jiao, A. Vasileff and S. Qiao, *Angew. Chem., Int. Ed.*, 2018, **57**, 7568–7579.

43 X. Wang, Y. Zheng, W. Sheng, Z. J. Xu, M. Jaroniec and S.-Z. Qiao, *Mater. Today*, 2020, **36**, 125–138.

44 S. Anantharaj, S. Noda, V. R. Jothi, S. Yi, M. Driess and P. W. Menezes, *Angew. Chem., Int. Ed.*, 2021, **60**, 18981–19006.

45 M. Lao, P. Li, Y. Jiang, H. Pan, S. X. Dou and W. Sun, *Nano Energy*, 2022, **98**, 107231.

46 J. Durst, A. Siebel, C. Simon, F. Hasché, J. Herranz and H. A. Gasteiger, *Energy Environ. Sci.*, 2014, **7**, 2255–2260.

47 X. Tian, P. Zhao and W. Sheng, *Adv. Mater.*, 2019, **31**, 1808066.

48 J. Zheng, W. Sheng, Z. Zhuang, B. Xu and Y. Yan, *Sci. Adv.*, 2016, **2**, e1501602.

49 W. Sheng, M. Myint, J. G. Chen and Y. Yan, *Energy Environ. Sci.*, 2013, **6**, 1509.

50 A. X. Nitish Govindarajan and K. Chan, *Science*, 2022, **375**, 6579.

51 H. Mistry, A. S. Varela, S. Kühl, P. Strasser and B. R. Cuenya, *Nat. Rev. Mater.*, 2016, **1**, 16009.

52 J. Zhang, S. Lu, Y. Xiang and S. P. Jiang, *ChemSusChem*, 2020, **13**, 2484–2502.

53 D. Liu, G. Xu, H. Yang, H. Wang and B. Y. Xia, *Adv. Funct. Mater.*, 2023, **33**, 2208358.

54 Y. Wang, X. Huang, H. Liu, W. Qiu, C. Feng, C. Li, S. Zhang, H. K. Liu, S. X. Dou and Z. M. Wang, *ACS Nano*, 2022, **16**, 5103–5130.

55 Y. Xiao, J. Ying, H. Liu and X. Yang, *Front. Chem. Sci. Eng.*, 2023, **17**, 1677–1697.

56 K. Guo, Z. He, S. Lu, P. Zhang, N. Li, L. Bao, Z. Yu, L. Song and X. Lu, *Adv. Funct. Mater.*, 2023, **33**, 2302100.

57 Q. Dang, Y. Sun, X. Wang, W. Zhu, Y. Chen, F. Liao, H. Huang and M. Shao, *Appl. Catal., B*, 2019, **257**, 117905.

58 X. Wang, Y. Zhang, J. Li, G. Liu, M. Gao, S. Ren, B. Liu, L. Zhang, G. Han, J. Yu, H. Zhao and F. Rosei, *Small Methods*, 2022, **6**, 2101470.

59 Y. Liu, J. Ma, S. Jia, C. Ma, P. Wu, L. Yang, L. Shen and G. Zhang, *Int. J. Hydrogen Energy*, 2025, **100**, 378–387.

60 D. Zhang, Z. Wang, X. Wu, Y. Shi, N. Nie, H. Zhao, H. Miao, X. Chen, S. Li, J. Lai and L. Wang, *Small*, 2021, **18**, 2104559.

61 C. Wang, J. Zhang, K. Miao, M. Long, S. Lai, S. Zhao and X. Kang, *Adv. Mater.*, 2024, **36**, 2400433.

62 C. Lin, Z. Huang, Z. Zhang, T. Zeng, R. Chen, Y. Tan, W. Wu, S. Mu and N. Cheng, *ACS Sustainable Chem. Eng.*, 2020, **8**, 16938–16945.

63 C. Tsounis, B. Subhash, P. V. Kumar, N. M. Bedford, Y. Zhao, J. Shenoy, Z. Ma, D. Zhang, C. Y. Toe, S. Cheong, R. D. Tilley, X. Lu, L. Dai, Z. Han and R. Amal, *Adv. Funct. Mater.*, 2022, **32**, 2203067.

64 Y. Li, K. Jiang, J. Yang, Y. Zheng, R. Hübner, Z. Ou, X. Dong, L. He, H. Wang, J. Li, Y. Sun, X. Lu, X. Zhuang, Z. Zheng and W. Liu, *Small*, 2021, **17**, 2102159.

65 Z. Yang, C. Zhao, Y. Qu, H. Zhou, F. Zhou, J. Wang, Y. Wu and Y. Li, *Adv. Mater.*, 2019, **31**, 1808043.

66 H. Cai, L. Xiong, B. Wang, D. Zhu, H. Hao, X. Yu, C. Li and S. Yang, *Chem. Eng. J.*, 2022, **430**, 132824.

67 J. Liu, Z. Wang, X. Wu, D. Zhang, Y. Zhang, J. Xiong, Z. Wu, J. Lai and L. Wang, *J. Mater. Chem. A*, 2022, **10**, 15395–15401.

68 X. Liu, Y. Jiao, Y. Zheng, K. Davey and S. Qiao, *J. Mater. Chem. A*, 2019, **7**, 3648–3654.

69 J. Yang, J. Feng, Y. Cao, Y. Xiao, L. Qiao, K. An, J. Yang, J. Peng, H. Pan and H. M. Cheng, *Adv. Funct. Mater.*, 2024, **34**, 2411081.

70 Y. Gu, B. Xi, R. Wei, Q. Fu, Y. Qain and S. Xiong, *Nano Lett.*, 2020, **20**, 8375–8383.

71 S. Fan, L. Shen, Y. Dong, G. Tian, S. Wu, G. Chang, C. Janiak, P. Wei, J. Wu and X. Yang, *J. Energy Chem.*, 2021, **57**, 189–197.

72 M. Etesami, M. T. Nguyen, T. Yonezawa, A. Tuantranont, A. Somwangthanaroj and S. Kheawhom, *Chem. Eng. J.*, 2022, **446**, 137190.

73 J. E. Park, Y. Sung and C. Choi, *J. Mater. Chem. A*, 2022, **10**, 20517–20524.

74 Y. Yu, Z. Zhu and H. Huang, *Adv. Mater.*, 2024, **36**, 2311148.

75 X. Yan, Y. Jia and X. Yao, *Chem. Soc. Rev.*, 2018, **47**, 7628–7658.

76 W. Li, D. Wang, Y. Zhang, L. Tao, T. Wang, Y. Zou, Y. Wang, R. Chen and S. Wang, *Adv. Mater.*, 2020, **32**, 1907879.

77 Y. Shen, P. Liu, J. Du, Y. Song, H. Cao, M. Zhao, P. Gao, B. Xu, J. Guo and Y. Wu, *Carbon*, 2020, **166**, 388–395.

78 Y. Chen, R. Ding, J. Li and J. Liu, *Appl. Catal., B*, 2022, **301**, 120830.

79 Q. Cheng, C. Hu, G. Wang, Z. Zou, H. Yang and L. Dai, *J. Am. Chem. Soc.*, 2020, **142**, 5594–5601.

80 S. Ye, F. Luo, Q. Zhang, P. Zhang, T. Xu, Q. Wang, D. He, L. Guo, Y. Zhang, C. He, X. Ouyang, M. Gu, J. Liu and X. Sun, *Energy Environ. Sci.*, 2019, **12**, 1000–1007.

81 X. Zheng, X. Zheng, M. Gao, Y. Liu, H. Pan and W. Sun, *Angew. Chem., Int. Ed.*, 2025, **64**, e202422062.

82 W. Yu, H. Huang, Y. Qin, D. Zhang, Y. Zhang, K. Liu, Y. Zhang, J. Lai and L. Wang, *Adv. Energy Mater.*, 2022, **12**, 2200110.

83 Y. Liang, Y. Li, H. Wang and H. Dai, *J. Am. Chem. Soc.*, 2013, **135**, 2013–2036.

84 A. K. Singh, N. Yasri, K. Karan and E. P. L. Roberts, *ACS Appl. Energy Mater.*, 2019, **2**, 2324–2336.

85 Y. Jiao, Y. Zheng, K. Davey and S. Qiao, *Nat. Energy*, 2016, **1**, 16130.

86 R. Huang, W. Liao, M. Yan, S. Liu, Y. Li and X. Kang, *J. Electrochem.*, 2023, **29**, 2203081.

87 G. Hasegawa, T. Deguchi, K. Kanamori, Y. Kobayashi, H. Kageyama, T. Abe and K. Nakanishi, *Chem. Mat.*, 2015, **27**, 4703–4712.

88 Y. Wang, Z. Tang, S. Shen and J. Yang, *New Carbon Mater.*, 2022, **37**, 321–336.

89 X. Cheng, C. Mao, J. Tian, M. Xia, L. Yang, X. Wang, Q. Wu and Z. Hu, *Angew. Chem., Int. Ed.*, 2024, **63**, e202401304.

90 X. Wang, Y. Jia, X. Mao, L. Zhang, D. Liu, L. Song, X. Yan, J. Chen, D. Yang, J. Zhou, K. Wang, A. Du and X. Yao, *Chem*, 2020, **6**, 2009–2023.

91 J. Tian, M. Xia, X. Cheng, C. Mao, Y. Chen, Y. Zhang, C. Zhou, F. Xu, L. Yang, X. Wang, Q. Wu and Z. Hu, *J. Am. Chem. Soc.*, 2024, **146**, 33640–33650.

92 J. Yang, J. Wang, R. Hübner, X. Tao, Y. Ren, Z. Zheng and W. Liu, *Adv. Energy Mater.*, 2024, **15**, 2404684.

93 J. Li, J. Liu, C. Chen, J. Guo, R. Bi, S. Chen, L. Zhang and M. Zhu, *Chem. Eng. J.*, 2022, **436**, 135186.

94 G. Ma, G. Ning and Q. Wei, *Carbon*, 2022, **195**, 328–340.

95 Y. Huang, X. Hu, Y. Li, X. Zhong, H. He, Z. Geng, S. Gan, W. Deng, G. Zou, H. Hou and X. Ji, *Adv. Funct. Mater.*, 2024, **34**, 2403648.

96 Y. Chen, X. Zheng, J. Cai, G. Zhao, B. Zhang, Z. Luo, G. Wang, H. Pan and W. Sun, *ACS Catal.*, 2022, **12**, 7406–7414.

97 X. Sun, X. Gao, J. Chen, X. Wang, H. Chang, B. Li, D. Song, J. Li, H. Li and N. Wang, *ACS Appl. Mater. Interfaces*, 2020, **12**, 48591–48597.

98 Y. Hou, M. Qiu, M. G. Kim, P. Liu, G. Nam, T. Zhang, X. Zhuang, B. Yang, J. Cho, M. Chen, C. Yuan, L. Lei and X. Feng, *Nat. Commun.*, 2019, **10**, 1392.

99 C. Yang, P. Yin, J. Liu, M. Chen, Q. Yan, Z. Wang, S. Xu, S. Chu, C. Cui, H. Ju, J. Zhu, Y. Lin, J. Shui and H. Liang, *Science*, 2021, **374**, 459–464.

100 Q. Yan, D. Wu, S. Chu, Z. Chen, Y. Lin, M. Chen, J. Zhang, X. Wu and H. Liang, *Nat. Commun.*, 2019, **10**, 4977.

101 Y. Li, J. Luo, P. Liu, L. Zhang, W. Song, Y. Wei, Z. Zhao, X. Zhang, J. Liu and Y. Sun, *J. Mater. Chem. A*, 2025, **13**, 11518–11529.

102 Y. Zhao, P. V. Kumar, X. Tan, X. Lu, X. Zhu, J. Jiang, J. Pan, S. Xi, H. Y. Yang, Z. Ma, T. Wan, D. Chu, W. Jiang, S. C. Smith, R. Amal, Z. Han and X. Lu, *Nat. Commun.*, 2022, **13**, 2430.

103 Q. Hu, G. Li, G. Li, X. Liu, B. Zhu, X. Chai, Q. Zhang, J. Liu and C. He, *Adv. Energy Mater.*, 2019, **9**, 1803867.

104 H. Wu, Z. Chen, Y. Wang, E. Cao, F. Xiao, S. Chen, S. Du, Y. Wu and Z. Ren, *Energy Environ. Sci.*, 2019, **12**, 2697–2705.

105 X. Chen, K. Niu, Z. Xue, X. Liu, B. Liu, B. Zhang, H. Zeng, W. Lv, Y. Zhang and Y. Wu, *Nanoscale Adv.*, 2022, **4**, 1639–1648.

106 M. Wang, C. Feng, W. Mi, M. Guo, Z. Guan, M. Li, H. Chen, Y. Liu and Y. Pan, *Adv. Funct. Mater.*, 2023, **34**, 2309474.

107 Z. Song, L. Zhang, K. DoyleDavis, X. Fu, J. Luo and X. Sun, *Adv. Energy Mater.*, 2020, **10**, 2001561.

108 X. Sun, S. Wang, Y. Hou, X. F. Lu, J. Zhang and X. Wang, *J. Mater. Chem. A*, 2023, **11**, 13089–13106.

109 H. Zhang, F. Wan, X. Li, X. Chen, S. Xiong and B. Xi, *Adv. Funct. Mater.*, 2023, **33**, 2306340.

110 P. Wang, Z. Wang, J. Mu, Y. Zhao, J. Xu, J. He, J. Jing and Y. Su, *Small*, 2025, **21**, 2502196.

111 F. Guo, T. J. Macdonald, A. J. Sobrido, L. Liu, J. Feng and G. He, *Adv. Sci.*, 2023, **10**, 2301098.

112 X. Wan, H. Wu, B. Guan, D. Luan and X. Lou, *Adv. Mater.*, 2019, **32**, 1901349.

113 M. Zhang, H. Li, J. Chen, F. Ma, L. Zhen, Z. Wen and C. Xu, *Adv. Funct. Mater.*, 2023, **33**, 2303189.

114 L. Zeng, Z. Zhao, Q. Huang, C. Zhou, W. Chen, K. Wang, M. Li, F. Lin, H. Luo, Y. Gu, L. Li, S. Zhang, F. Lv, G. Lu, M. Luo and S. Guo, *J. Am. Chem. Soc.*, 2023, **145**, 21432–21441.

115 C. Li, Y. Ji, Q. Wei, Z. Liu, Y. Wu, L. Chen, D. Han, L. Niu, C. Tao and D. Qin, *ACS Appl. Energy Mater.*, 2023, **6**, 997–1007.

116 J. Hao, F. Wei, X. Zhang, L. Li, C. Zhang, D. Liang, X. Ma and P. Lu, *Nanoscale Res. Lett.*, 2021, **16**, 130.

117 X. Bao, Y. Gong, Y. Chen, H. Zhang, Z. Wang, S. Mao, L. Xie, Z. Jiang and Y. Wang, *J. Mater. Chem. A*, 2019, **7**, 15364–15370.

118 X. Luo, P. Yuan, H. Xiao, S. Li, J. Luo, J. Li, W. Lai, Y. Chen and D. Li, *ACS Appl. Mater. Interfaces*, 2024, **16**, 26044–26056.

119 R. Zhang, Y. Li, X. Zhou, A. Yu, Q. Huang, T. Xu, L. Zhu, P. Peng, S. Song, L. Echegoyen and F. Li, *Nat. Commun.*, 2023, **14**, 2460.

120 Y. Hong, S. C. Cho, S. Kim, H. Jin, J. H. Seol, T. K. Lee, J. K. Ryu, G. M. Tomboc, T. Kim, H. Baik, C. Choi, J. Jo, S. Jeong, E. Lee, Y. Jung, D. Ahn, Y. Kim, S. Yoo, S. Lee and K. Lee, *Adv. Energy Mater.*, 2024, **14**, 2304269.

121 Z. Zeng, S. Küspert, S. E. Balaghi, H. E. M. Hussein, N. Ortlieb, M. Knäbbeler-Buß, P. Hügenell, S. Pollitt, N. Hug, J. Melke and A. Fischer, *Small*, 2023, **19**, 2205885.

122 Y. Xiao, J. Ying, J. Chen, Y. Dong, X. Yang, G. Tian, J. Wu, C. Janiak, K. I. Ozoemena and X. Yang, *Chem. Mat.*, 2022, **34**, 3705–3714.

123 S. Zhang, X. F. Lu, Z. Wu, D. Luan and X. W. Lou, *Angew. Chem., Int. Ed.*, 2021, **60**, 19068–19073.

124 Y. Xu, J. Du, J. Jiang, Y. Miao, Z. Zhuang, Z. Liu, Y. Yan, R. Pan, J. Yang, M. Wang, S. Gu, L. Kang and D. Wang, *Angew. Chem., Int. Ed.*, 2025, **64**, e202502227.

125 J. Chen, M. Aliasgar, F. B. Zamudio, T. Zhang, Y. Zhao, X. Lian, L. Wen, H. Yang, W. Sun, S. M. Kozlov, W. Chen and L. Wang, *Nat. Commun.*, 2023, **14**, 1711.

126 G. Li, H. Xu, X. Lu, J. Feng, Y. Tong and C. Su, *Nanoscale*, 2013, **5**, 4056.

127 Y. Wu, B. Xiao, K. Liu, S. Wang, Y. Hou, X. F. Lu and J. Zhang, *Electrochem. Energy Rev.*, 2025, **8**, 2.

128 C. Zhu, H. Wang and C. Guan, *Nanoscale Horiz.*, 2020, **5**, 1188–1199.

129 M. B. Kale, R. A. Borse, A. Gomaa Abdelkader Mohamed and Y. Wang, *Adv. Funct. Mater.*, 2021, **31**, 2101313.

130 C. Zhou, K. Ma, Z. Zhuang, M. Ran, G. Shu, C. Wang, L. Song, L. Zheng, H. Yue and D. Wang, *J. Am. Chem. Soc.*, 2024, **146**, 21453–21465.

131 Z. Li, W. Niu, Z. Yang, A. Kara, Q. Wang, M. Wang, M. Gu, Z. Feng, Y. Du and Y. Yang, *Energy Environ. Sci.*, 2020, **13**, 3110–3118.

132 Q. Yang, H. Liu, P. Yuan, Y. Jia, L. Zhuang, H. Zhang, X. Yan, G. Liu, Y. Zhao, J. Liu, S. Wei, L. Song, Q. Wu, B. Ge, L. Zhang, K. Wang, X. Wang, C.-R. Chang and X. Yao, *J. Am. Chem. Soc.*, 2022, **144**, 2171–2178.

133 J. Ji, Z. Li, C. Hu, Y. Sha, S. Li, X. Gao, S. Zhou, T. Qiu, C. Liu, X. Su, Y. Hou, Z. Lin, S. Zhou, M. Ling and C. Liang, *ACS Appl. Mater. Interfaces*, 2020, **12**, 40204–40212.

134 J. Ji, Y. Zhang, L. Tang, C. Liu, X. Gao, M. Sun, J. Zheng, M. Ling, C. Liang and Z. Lin, *Nano Energy*, 2019, **63**, 103849.